

**COMPUTATION OF RHEOLOGICAL NANOFLUID COATING BOUNDARY LAYER  
TRANSPORT WITH CONVECTIVE WALL HEATING**

***M.J Uddin<sup>1\*</sup>, O. Anwar Bég<sup>2</sup> and Sireetorn Kuharat<sup>2</sup>***

<sup>1</sup>Professor, Dept. of Mathematics, and Convener, Office of Research, American International University-Bangladesh, Kuril, Dhaka 1229, Bangladesh.

**\*Corresponding author - Email: [drjashim@aiub.edu](mailto:drjashim@aiub.edu), [jashim\\_74@yahoo.com](mailto:jashim_74@yahoo.com)**

<sup>2</sup>Professor and Director- MPESG, Corrosion/Coating Lab, 3-08, Aeronautical & Mechanical Engineering Dept., SEE Building, Salford University, Manchester, M54WT, UK.

Email- [O.A.Beg@salford.ac.uk](mailto:O.A.Beg@salford.ac.uk)

<sup>2</sup>Lecturer in Aeronautical Engineering, MPESG, Corrosion/Coating Lab, 3-08, Aeronautical & Mechanical Engineering Dept., SEE Building, Salford University, Manchester, M54WT, UK.

Email: [S.Kuharat2@salford.ac.uk](mailto:S.Kuharat2@salford.ac.uk)

**ABSTRACT:** *Non-Newtonian nanofluids offer significant advantages in thermal enhancement in a variety of applications including in numerous areas of engineering including solar collectors and nano-coating manufacturing processes. When combined with porous media, yet further benefits can be gained in for example flow and heat transfer manipulation in nano-rheological coating extrusion. Motivated by exploring this industrial application, to furnish a deeper understanding of the rheological and nanoscale effects of such fluids in porous media, we examine the steady two dimensional (2-D) laminar buoyancy-driven boundary layer flow of power-law nanofluids along vertically upward surface adjacent to an isotropic Darcian porous filtration medium. Buongiorno's two-component nanofluid model is deployed. Scaling group transformations followed by dimensional analysis is used to developed group invariants and hence the primitive conservation equations for momentum, heat and NVF are transformed from partial differential equations into ordinary differential equations with associated wall and free stream boundary conditions. The reduced nonlinear boundary value problem has been solved computationally with the stable, rapidly convergent Runge-Kutta-Fehlberg fourth-fifth order numerical method available in the symbolic platform, **Maple 18**. Verification of the methodology with earlier Blottner finite difference computations in the literature for the special case of  $N_c = N_d = 0$  is included. It is found that the reduced Nusselt number increases with convective-conduction parameter,  $N_c$ , while it is suppressed with increasing power-law index,  $n$ , and thermophoresis parameter,  $N_t$ . The reduced Sherwood number is enhanced with Lewis number,  $Le$  and convective-diffusion parameter,  $N_d$  whereas it is substantially depleted with increasing power-law index,  $n$ . Strong boundary layer flow acceleration is induced with higher  $N_c$  values. Temperature is also strongly boosted with an elevation in power-law index and both convection-conduction  $N_c$  and convection-diffusion  $N_d$  parameters. Dilatant i. e. shear-thickening nanofluids ( $n > 1$ ) are observed to achieve the best thermal enhancement. The novelty of the current work is the rigorous analysis of different rheological and wall heating and nanoparticle volume fraction effects on nano-polymer coating flows which significantly extends existing studies.*

**KEYWORDS:** *Lie symmetry group transformation; Power law nanofluid; Porous media; Convective wall boundary conditions; thermal enhancement, nano-coating manufacture, MAPLE 18.*

## 1. INTRODUCTION

Nanofluid dynamics has rapidly evolved into a substantial sub-area of thermofluid mechanics, stimulated by an astonishing range of applications. A nanofluid is defined as a viscous fluid containing nanoparticles with dimensions of around 100 nm. These fluids, introduced by Choi [1], have achieved improved thermophysical properties including thermal diffusivity, kinematic viscosity, heat, and nanoparticle volume fraction gradient at the wall significantly elevating the performance of traditional carrier fluids (e. g. oil, water etc). Recently nanofluids have been deployed in medical engineering [2-5], rocket propulsion [6], astronomical heat pipes [7], solar collectors [8], thermosyphons [9] and micro-channels [10], to quote only a few applications. Extensive studies of both Newtonian and non-Newtonian nanofluids in porous environment reported in the literature owing to relevance in materials processing and biotechnology. Ellahi *et al.* [11] studied non-Newtonian nanofluids applications in for example polymer melts. Many rheological models have been used for nanofluids and many numerical techniques employed to solve the boundary value problems formulated. Empirical studies have also been reported. Nield [12] considered analytically the onset of thermal convection in a porous medium saturated with power-law nanofluids. Hojjat *et al.* [13] conducted detailed experiments on aluminium, copper, and titanium oxide nanoparticles in an aqueous mixer of carboxymethyl cellulose, observing pseudoplastic (shear-thinning) rheological behaviour. They derived a novel correlation for heat transfer rates as function of power-law index, Reynolds and Prandtl numbers. Rana *et al.* [14] applied a variational finite element method to study deformation effects in nonlinear viscoelastic nanofluid flow as a simulation of nano-polymer manufacturing extrusion dynamics. They observed that viscoelasticity enhances thermal diffusion in such flows. Rashad *et al.* [15] applied an efficient numerical method (Keller's implicit difference box method) to investigate wall mass flux effects on nanofluid power-law transport in porous media. Sheu *et al.* [16] examined the hydrodynamic stability of convective flow of Oldroyd-B viscoelastic nanofluid. Chand and Rana [17] used the Rivlin Ericksen differential fluid model to simulate the impacts of kinematics viscoelasticity on the stability of rheological nanofluid flow.

Multi-physical transport in porous media has also advanced into a considerable sub-discipline of fluid mechanics over the last couple of decades. An outstanding review of progress in this field has been provided by Kaviani [18] in which combined modes of thermal transport have also been addressed i.e., conduction, convection, and radiation, in addition to viscous percolation fluid dynamics. Porous media flow modeling continues to stimulate interest in the 21<sup>st</sup> century owing to ever-growing needs in manufacturing (filtration) systems, energy optimization, biotechnological liquid processing (linctuses, creams, lubricants), drying and chemical engineering fluidized bed technologies. The many methodologies for simulating porous media flows have been lucidly summarized by Adler and Brenner [19] and include geometric models, spatially periodic porous media models, volume averaging, reconstructed porous media and drag force models. Further applications of porous media transport phenomena include combustion systems [20], electro-conductive polymer processing [21], paint and colloid fabrication [22] and geophysics [23]. Many *non-Newtonian* models have been explored in recent years for flow in such diverse areas. We mention here Eringen micro-morphic fluids [24, 25], Stokesian couple stress (polar) fluids [26], empirical rheological foam models [27], upper-convected Maxwell (UCM) models [28], and memory fluids [29]. These studies have employed and/or extended the fundamental Darcy drag-force approach popularized by Cheng and Minkowycz [30] which is valid for low Reynolds number, viscous-dominated flows. In recent years the *range* of non-Newtonian models deployed has been considerably widened to simulate characteristics of different working fluids ranging more accurately from crude oils to physiological liquids. Interesting communications include Mahmoud [31] who used an Ostwald-deWaele power-law model to simulate polymer heat transfer from a cone. Tripathi and Bég [32] employed a magnetic-polar model for gastric flow control simulations. Bég *et al.* [33] used the Nakamura-Sawada bi-viscosity rheological model to study targeted drug transport in tissue. Further models successfully utilized models include Reiner-Rivlin second grade viscoelastic fluids [34], Reiner-Rivlin-Fosdick third grade liquids [35], electromagnetic micropolar biofluids [36], Walters-B elastoviscous fluids [37], Bingham plastics (yield stress models) [38], fractional Maxwell fluids [39] and Marble-Drew fluid-particle suspension models [40]. All these models allow the construction of robust boundary value problems which can be tackled analytically or numerically. The success of the Nield-Kuznetsov *Newtonian* nanofluid model [41], which itself is an extension of the now classical Cheng-Minkowycz boundary layer problem [30] has naturally encouraged generalizations to *non-Newtonian nanofluid* models in porous (permeable) media.

Based on the literature stated above, it is evident that no research has been thus far conducted on the *coating boundary layer flow of power law nanofluids in a movable free stream over a non-iso-concentration substrate surface embedded in a saturated Darcian medium, considering both thermal and nanoparticle volume fraction (NVF) convective wall boundary conditions*. Hence the objective of the present paper is to analyse flow, heat transfer and NVF transfer behaviour of relevance to wall characteristics. This regime is important in nano-polymer coating manufacture. The present article deploys Lie algebra group scaling transformations to generate a well-posed nonlinear boundary value problem. **MAPLE 18** shooting quadrature is deployed to achieve robust numerical solutions. The influence of emerging thermophysical parameters on the velocity, temperature and NVF distributions is visualized graphically and key connections to implications for nano-polymer coating systems are explained. Validation with previous studies neglecting convective wall heating is also included and future pathways.

## 2. MATHEMATICAL NANO-POLYMER COATING FLOW MODEL

In the present study we examine coating boundary layer flow of power law nanofluids in a movable free stream over a non-iso-concentration substrate surface embedded in a saturated Darcian medium, considering both thermal and nanoparticle volume fraction (NVF) convective wall boundary conditions. The physical model in a rectangular coordinate system reference frame is depicted in **Fig. 1**. The following assumptions are made:

- i. The is incompressible time-independent laminar rheological nanofluid flow.
- ii. The porous media is isotropic and homogenous.
- iii. The Darcy law is utilized which is valid for low Reynolds numbers up to approximately 10.
- iv. The Ostwald-DeWaele power-law non-Newtonian model is adopted.
- v. Thermophysical properties are constant.
- vi. The wall boundary follows convective boundary condition.
- vii. The Buongiorno nanoscale model is implemented which features thermophoretic body force and Brownian dynamics.
- viii. Nanofluid properties are assumed invariant except density.
- ix. Boussinesq approximation is adopted.

The Darcy velocity components are symbolised as  $\bar{u}$  and  $\bar{v}$ , respectively. Tortuosity, dispersion, and stratification effects are ignored for the porous medium. is deployed for

rheological features of the nanofluid. This model, although simple, successfully captures the shear-thinning (pseudoplastic) or shear-thickening (dilatant) features exhibited by different nanofluid suspensions.

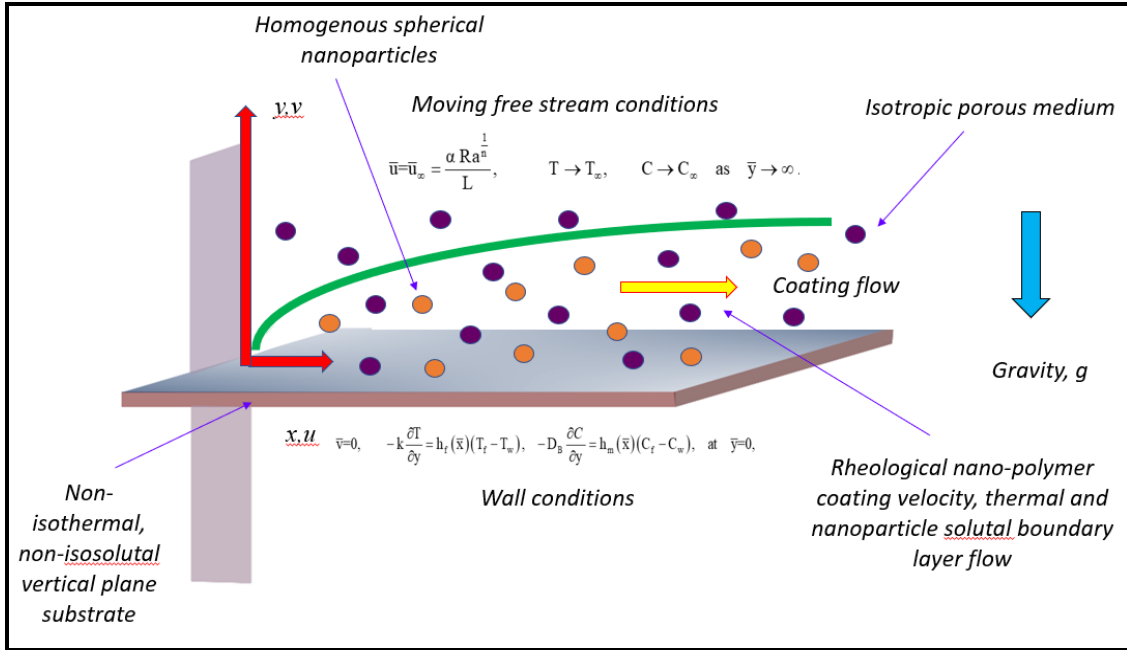


**Fig.1.** Physical model for nano-polymer coating of a substrate

The nano-polymer is a dilute suspension. The nanofluid in the far field (edge of boundary layer) moves with a uniform free stream velocity,  $\bar{u}_\infty$ . Hot nanofluid in the coating is at temperature,  $T_f$  at the wall (substrate) and produces a thermal convection coefficient,  $h_f$ . Similarly, NVF  $C_f$ , exceeds the volume fraction at the wall,  $C_w$ , which yields a NVF coefficient,  $h_m$ . Temperature  $T_w$  and NVF  $C_w$  at the wall are in excess of the ambient values  $T_\infty$ ,  $C_\infty$  respectively. Free convective flow is permitted to happen between the substrate surface and the nanofluid coating. Based on the above assumptions, the primitive conservation equations for mass, momentum, and NVF, following [Gorla and Chamkha 43] and extending take the form:

$$\frac{\partial \bar{u}}{\partial \bar{x}} + \frac{\partial \bar{v}}{\partial \bar{y}} = 0, \quad (1)$$

$$\frac{\partial \bar{u}^n}{\partial \bar{y}} = \frac{(1 - C_\infty) g \rho_{f_\infty} K_o \beta}{K} \frac{\partial T}{\partial \bar{y}} - \frac{(\rho_p - \rho_{f_\infty}) g K_o}{K} \frac{\partial C}{\partial \bar{y}}, \quad (2)$$

$$\bar{u} \frac{\partial T}{\partial \bar{x}} + \bar{v} \frac{\partial T}{\partial \bar{y}} = \alpha \frac{\partial^2 T}{\partial \bar{y}^2} + \tau \left[ D_B \frac{\partial T}{\partial \bar{y}} \frac{\partial C}{\partial \bar{y}} + \left( \frac{D_T}{T_\infty} \right) \left( \frac{\partial T}{\partial \bar{y}} \right)^2 \right], \quad (3)$$

$$\bar{u} \frac{\partial C}{\partial \bar{x}} + \bar{v} \frac{\partial C}{\partial \bar{y}} = D_B \frac{\partial^2 C}{\partial \bar{y}^2} + \left( \frac{D_T}{T_\infty} \right) \frac{\partial^2 T}{\partial \bar{y}^2}, \quad (4)$$

Here  $\tau = \frac{(\rho C)_p}{(\rho C)_f}$  : (ratio of nanoparticles heat capacity to base fluid heat capacity) and

$\alpha = \frac{k}{(\rho C)_f}$  (thermal diffusivity). Following Aziz [42], the wall and free stream boundary

conditions are:

$$\begin{aligned} \bar{v} = 0, \quad -k \frac{\partial T}{\partial \bar{y}} = h_f(\bar{x})(T_f - T_w), \quad -D_B \frac{\partial C}{\partial \bar{y}} = h_m(\bar{x})(C_f - C_w), \quad \text{at } \bar{y} = 0, \\ \bar{u} = \bar{u}_\infty = \frac{\alpha Ra^n}{L}, \quad T \rightarrow T_\infty, \quad C \rightarrow C_\infty \quad \text{as } \bar{y} \rightarrow \infty. \end{aligned} \quad (5)$$

In the momentum eqn. (2), the power-law rheological index for the nanofluid controls the nature of the fluid rheology. When  $n=1$  we recover Newtonian fluid for which the dynamic viscosity  $\mu = K$ . This version of the present model agrees exactly with the earlier study of Gorla and Chamkha [43]. For  $n<1$  the model signifies shear-thinning fluids (pseudoplastic) and for  $n>1$  the model signifies shear thickening fluids (dilatant). Chen *et al.* [44] have described in detail the practical nature of nanofluids exhibiting these characteristics. Their experiments have demonstrated that *shear-thinning* performance of nanofluids is a function of the effective particle concentration, the shear rate range, and the viscosity of the carrier liquid (e. g. water, ethylene glycol etc). They have further identified that for pseudoplastic fluids, the shear rate is reduced with rising volume fraction, aggregate size, or base fluid viscosity. In the present simulations, we shall address these findings and further consider dilatancy behaviour.

### 2.1. Non-dimensional version of nanofluid transport model

Let us introduce rescaled variables as defined below:

$$x = \frac{\bar{x}}{L}, \quad y = \frac{\bar{y}}{L} Ra^{\frac{1}{2n}}, \quad u = \frac{L\bar{u}}{\alpha Ra^{\frac{1}{n}}}, \quad v = \frac{L\bar{v}}{\alpha Ra^{\frac{1}{2n}}}, \quad \theta = \frac{T - T_\infty}{T_f - T_\infty}, \quad \varphi = \frac{C - C_\infty}{C_f - C_\infty}, \quad (6)$$

Furthermore, a dimensional stream function,  $\psi$ , given below is applied:

$$u = \frac{\partial \psi}{\partial y}, \quad v = -\frac{\partial \psi}{\partial x} \quad (7)$$

Introduction of the non-dimensional variables (6) and Eqn. (7) into Eqns. (2)-(5) eliminates the streamwise similarity variable and generates the following three coupled nonlinear boundary layer equations for momentum, energy, and concentration:

$$n \left( \frac{\partial \psi}{\partial y} \right)^{n-1} \frac{\partial^2 \psi}{\partial y^2} - \frac{\partial \theta}{\partial y} + Nr \frac{\partial \varphi}{\partial y} = 0, \quad (8)$$

$$\frac{\partial \psi}{\partial y} \frac{\partial \theta}{\partial x} - \frac{\partial \psi}{\partial x} \frac{\partial \theta}{\partial y} = \frac{\partial^2 \theta}{\partial y^2} + Nb \frac{\partial \theta}{\partial y} \frac{\partial \varphi}{\partial y} + Nt \left( \frac{\partial \theta}{\partial y} \right)^2, \quad (9)$$

$$\frac{\partial \psi}{\partial y} \frac{\partial \varphi}{\partial x} - \frac{\partial \psi}{\partial x} \frac{\partial \varphi}{\partial y} = \frac{1}{Le} \frac{\partial^2 \varphi}{\partial y^2} + \frac{Nt}{Nb} \frac{1}{Le} \frac{\partial^2 \varphi}{\partial y^2}, \quad (10)$$

The boundary conditions (5) transform to:

$$\frac{\partial \psi}{\partial x} = 0, \quad \frac{\partial \theta}{\partial y} = \frac{-h_f(x)L}{kRa^{\frac{1}{2n}}}(1-\theta), \quad \frac{\partial \varphi}{\partial y} = \frac{-h_m(x)L}{D_B Ra^{\frac{1}{2n}}}(1-\varphi) \quad \text{at } y=0, \quad (11)$$

$$\frac{\partial \psi}{\partial y} \rightarrow 1, \quad \theta \rightarrow 0, \quad \varphi \rightarrow 0 \quad \text{as } y \rightarrow \infty.$$

The mass conservation Eqn. (1) is satisfied automatically. The thermophysical control parameters featured in Eqns. (8)-(10) i. e.  $Nr$ ,  $Nb$ ,  $Nt$ ,  $Ra$  and  $Le$  signify the buoyancy ratio, the Brownian motion parameter, thermophoresis parameter, porous medium Rayleigh number and Lewis number, respectively. These parameters take the following mathematical definitions:

$$\begin{aligned}
Nr &= \frac{(\rho_p - \rho_{f_\infty})(C_f - C_\infty)}{\rho_{f_\infty} \beta (T_f - T_\infty)(1 - \varphi_\infty)}, Nb = \frac{(\rho C)_p D_B (C_f - C_\infty)}{(\rho C)_f \alpha}, Nt = \frac{(\rho C)_p D_T (T_f - T_\infty)}{(\rho C)_f \alpha T_\infty}, \\
Ra &= \frac{(1 - C_\infty) g \rho_{f_o} K_o \beta (T_f - T_\infty) L^n}{\mu \alpha^n}, \quad Le = \frac{\alpha}{D_B}.
\end{aligned} \tag{12}$$

Inspection of Eqn. (12) reveals that the only dimensionless hydrodynamic number featuring the power-law rheological index  $n$  is the porous medium Rayleigh number,  $Ra$ . However,  $n$  does feature in the nonlinear stream function gradient term in Eqn. (8) and furthermore arises in the denominators in the wall temperature and nanoparticle volume fraction wall convective conditions, specified in eqn. (11).

## 2.2 Symmetry analysis

The non-dimensional boundary value problem although significantly simpler than the primitive boundary layer equations, still may be further simplified. Invariant transformations of the dimensionless transport equations can be established. These are achievable via a spectrum of techniques such as separation of variables. In the present study we elect to employ a more comprehensive strategy based on the *Lie group algebraic method*. This approach is very attractive for nonlinear partial differential equations, as studied in the present article. The most important Lie groups are the three families of ‘‘classical groups’’. Extensive details of these methods are documented in Seshadri and Na [45] and Ibragimov [46]. Lie group scaling has emerged as a powerful technique in recent years in multi-physical fluid dynamics and thermophysics. Recent applications of this method include theoretical studies of heat generating nanofluid gels [47], turbulent boundary layer scaling [48], reactive flows [49], premixed combustion flows [50], nanofluid flow in porous media [51] and magnetohydrodynamic flows [52]. Following Aziz *et al.* [53], we use the following transformations.

$$\Gamma : x^* = x e^{\epsilon \alpha_1}, \quad y^* = y e^{\epsilon \alpha_2}, \quad \psi^* = \psi e^{\epsilon \alpha_3}, \quad \theta^* = \theta e^{\epsilon \alpha_4}, \quad \varphi^* = \varphi e^{\epsilon \alpha_5}, \quad h_f^* = h_f e^{\epsilon \alpha_6}, \quad h_m^* = h_m e^{\epsilon \alpha_7}, \tag{13}$$

Here  $\epsilon, \alpha_1 \dots \alpha_7$  are constants with at least one non-zero value. Transformations applied to Eqn. (13) converts:

the coordinates  $(x, y, \psi, \theta, \varphi, h_f, h_m)$  to  $(x^*, y^*, \psi^*, \theta^*, \varphi^*, h_f^*, h_m^*)$ .

The equations will be *invariant* if the structural form of transformation before and after is the same ([45, 46, 47, 49-53]). The equations (11) will be invariant if:

$$\alpha_5 = \alpha_4 = 0, \quad \alpha_1 = 2\alpha_2, \quad \alpha_3 = \alpha_2, \quad \alpha_6 = \alpha_7 = -\alpha_2. \quad (14)$$

### 2.3. Absolute Invariants

Proceeding with the analysis, the transformations in Eqn. (13) become:

$$\Gamma: x^* = xe^{2\epsilon\alpha_2}, \quad y^* = ye^{\epsilon\alpha_2}, \quad \psi^* = \psi e^{\epsilon\alpha_2}, \quad \theta^* = \theta, \quad \varphi^* = \varphi, \quad h_f^* = h_f e^{-\epsilon\alpha_2}, \quad h_m^* = h_m e^{-\epsilon\alpha_2}. \quad (15)$$

With the values of  $\alpha_i$ , the transformations can be readily expanded using Taylor series. Subsequently *characteristic equations* are applied and solved to derive the similarity transformations.

$$\frac{1}{2\alpha_2} \frac{dx}{x} = \frac{1}{\alpha_2} \frac{dy}{y} = \frac{1}{\alpha_2} \frac{d\psi}{\psi} = \frac{d\theta}{0} = \frac{d\varphi}{0} = \frac{1}{-\alpha_2} \frac{dh_f}{h_f} = \frac{1}{-\alpha_2} \frac{dh_m}{h_m}, \quad \alpha_2 \neq 0. \quad (16)$$

Solving (16), we get the following *absolute invariants*:

$$\eta = \frac{y}{x^{\frac{1}{2}}}, \quad \psi = x^{\frac{1}{2}} f(\eta), \quad \theta = \theta(\eta), \quad \varphi = \varphi(\eta), \quad h_f = (h_f)_o \frac{1}{x^{\frac{1}{2}}}, \quad h_m = (h_m)_o \frac{1}{x^{\frac{1}{2}}} \quad (17)$$

Here  $(h_f)_o$ ,  $(h_m)_o$  are constant heat, mass transfer coefficient and  $\eta$  denotes the similarity variable.

### 2.4. Self-Similar Transport Equations

Introducing Eq. (17) into Eqns. (8)-(11), we arrive at:

$$nf^{(n-1)} f'' - \theta' + Nr \varphi' = 0, \quad (18)$$

$$\theta'' + \frac{1}{2} f \theta' + Nb \varphi' \theta' + Nt \theta'^{(2)} = 0, \quad (19)$$

$$\varphi'' + \frac{Nt}{Nb} \theta'' + \frac{1}{2} Lef \varphi' = 0, \quad (20)$$

The finalized version of the boundary conditions (11) emerges as:

$$f(0) = 0, \theta'(0) = -Nc[1 - \theta(0)], \varphi'(0) = -Nd[1 - \varphi(0)], f'(\infty) - 1 = \theta(\infty) = \varphi(\infty) = 0. \quad (21)$$

Here  $Nc = (h_f)_o L / k Ra^{2n}$  is the convection-conduction parameter while  $Nd = (h_m)_o L / D_B Ra^{2n}$  is the convection-diffusion parameter. Note that for a *Newtonian* fluid ( $n = 1$ ) flowing along an *isothermal* and *iso-solutal* substrate ( $Nc \rightarrow \infty, Nd \rightarrow \infty$ ) in the quiescent free stream, the present generalized model retracts to exactly the model studied by Gorla and Chamkha [43]. Further, for a stationary free stream in the absence of nanofluid parameters, and for  $Nc \rightarrow \infty, Nd \rightarrow \infty$  the current model contracts to exactly that studied earlier by Chen and Chen [54]. In practical applications relevant to materials processing and energy systems, the principal wall gradient characteristics of physical interest are the local Nusselt number ( $Nu_{\bar{x}}$ ) i.e. dimensionless heat transfer rate to the substrate from the coating flow and local Sherwood number ( $Sh_{\bar{x}}$ ) i.e. dimensionless nanoparticle species transfer rate to the substrate from the coating boundary layer flow, which may be defined, respectively as:

$$Nu_{\bar{x}} = \frac{-\bar{x}}{(T_w - T_\infty)} \left( \frac{\partial T}{\partial y} \right)_{\bar{y}=0}, \quad Sh_{\bar{x}} = \frac{-\bar{x}}{(C_w - C_\infty)} \left( \frac{\partial C}{\partial y} \right)_{\bar{y}=0}. \quad (22)$$

Using Eqns. (6) and (17), we obtain:

$$Ra_{\bar{x}}^{-1/2n} Nu_{\bar{x}} = -\theta'(0), \quad Ra_{\bar{x}}^{-1/2n} Sh_{\bar{x}} = -\varphi'(0). \quad (23)$$

where  $Ra_{\bar{x}} = (1 - C_\infty) g \rho_{fo} K_o \beta \Delta T L^n \bar{x}^n / K \alpha^n$  is the local Rayleigh number. According to Nield and Kuznetsov [41], the *reduced local Nusselt number* and *reduced local Sherwood number* can be represented as follows:

$$Nur = Ra_{\bar{x}}^{-1/2n} Nu_{\bar{x}} = -\theta'(0), \quad Shr = Ra_{\bar{x}}^{-1/2n} Sh_{\bar{x}} = -\varphi'(0) \quad (24)$$

### 3. NUMERICAL SIMULATION AND VALIDATION

The set of self-similar coupled nonlinear ordinary differential boundary layer eqns. Eqns. (18) - (20) subject to the prescribed boundary conditions (21) have been solved computationally using the Runge-Kutta-Fehlberg fourth-fifth order numerical technique

available in the symbolic software **Maple 18**. MAPLE 18 is an excellent symbolic software with many libraries of built in ready-to-use numerical solvers for ordinary and partial differential problems. This approach allows very accurate estimation of the stream function, temperature, and nanoparticle concentration functions. The appropriate velocity is then computed in a sub-iteration loop. This approach has been extensively implemented recently in many applications including oxygen diffusion in capillaries [55] and spin coating of aerospace components [56]. The robustness and stability of this numerical method is therefore well established- it is highly adaptive since it adjusts the quantity and location of grid points during iteration and thereby constrains the local error within acceptable specified bounds. Many different wall boundary conditions which arise nano-materials coating process fluid dynamics can be easily accommodated. The stepping formulae although designed for nonlinear problems, are even more efficient for any order of linear differential equation and are summarized below [56]:

$$k_0 = f(x_i, y_i), \quad (25)$$

$$k_1 = f\left(x_i + \frac{1}{4}h, y_i + \frac{1}{4}hk_0\right), \quad (26)$$

$$k_2 = f\left(x_i + \frac{3}{8}h, y_i + \left(\frac{3}{32}k_0 + \frac{9}{32}k_1\right)h\right), \quad (27)$$

$$k_3 = f\left(x_i + \frac{12}{13}h, y_i + \left(\frac{1932}{2197}k_0 - \frac{7200}{2197}k_1 + \frac{7296}{2197}k_2\right)h\right), \quad (28)$$

$$k_4 = f\left(x_i + h, y_i + \left(\frac{439}{216}k_0 - 8k_1 + \frac{3860}{513}k_2 - \frac{845}{4104}k_3\right)h\right), \quad (29)$$

$$k_5 = f\left(x_i + \frac{1}{2}h, y_i + \left(-\frac{8}{27}k_0 + 2k_1 - \frac{3544}{2565}k_2 + \frac{1859}{4101}k_3 - \frac{11}{40}k_4\right)h\right), \quad (30)$$

$$y_{i+1} = y_i + \left(\frac{25}{216}k_0 + \frac{1408}{2565}k_2 + \frac{2197}{4101}k_3 - \frac{1}{5}k_4\right)h, \quad (31)$$

$$z_{i+1} = z_i + \left(\frac{16}{135}k_0 + \frac{6656}{12825}k_2 + \frac{28561}{56430}k_3 - \frac{9}{50}k_4 + \frac{2}{55}k_5\right)h. \quad (32)$$

Here  $y$  denotes the fourth *order* Runge-Kutta phase and  $z$  is the *fifth order* Runge-Kutta phase. An estimate of the error is achieved by subtracting the two values obtained. If the

error exceeds a specified threshold, the results can be re-calculated using a smaller step size. The approach to estimating the new step size is shown below:

$$h_{new} = h_{old} \left( \frac{\varepsilon h_{old}}{2|z_{i+1} - y_{i+1}|} \right)^{1/4}. \quad (33)$$

The free stream conditions in (21) have been substituted by a finite value of 5 for the transverse similarity variable,  $\eta_{max}$ . The choice of  $\eta_{max}$  confirms that all simulated results meet the potential boundary conditions asymptotically. This issue has been emphasized in the context of power-law non-Newtonian flows by Denier and Dabrowski [57]. For *dilatant nanofluids* ( $n > 1$ ) it is imperative that shooting solutions obey the correct form of asymptotic fall in the free stream. The local rate of heat transfer and nanoparticles volume fraction mass transfer rate are, respectively, measured by *Nur* and *Shr*. To verify the correctness of the numerical method, we have benchmarked special cases of the generalized model here with Chen and Chen [54] and Gorla and Chamkha [43]. The comparisons are provided in **Tables 1-3**.

**Table 1** Evaluation of  $-\theta'(0)$  for various  $n$ .

$n$	Chen and Chen [54] $-\theta'(0)$	Our results $-\theta'(0)$
0.5	0.3768	0.37684
0.8	0.4838	0.48389
1.0	0.4437	0.44366
1.5	0.4752	0.47518
2.0	0.4938	0.49377

**Table 2:** Comparison of  $-\theta'(0)$  and  $-\varphi'(0)$  when  $Nc = Nd \rightarrow \infty$ ,  $n=1$ ,  $Nb=0.3$ ,  $Nt=0.1$ ,  $Le=10$ .

	$-\theta'(0)$	$-\varphi'(0)$
--	---------------	----------------

$Nr$	Gorla and Chamkha [43]	Our results	Gorla and Chamkha [43]	Our results
0.1	0.3297846	0.3294	1.619866	1.6178
0.2	0.3227547	0.3221	1.556346	1.5543
0.3	0.3149958	0.3144	1.489373	1.4878
0.4	0.3072273	0.3063	1.419391	1.4178
0.5	0.2980915	0.2976	1.344729	1.3435

**Table 3:** Comparison of  $-\theta'(0)$  and  $-\varphi'(0)$  when  $Nc = Nd \rightarrow \infty$ ,  $n=1$ ,  $Nt=0.1$ ,  $Nr=0.5$ ,  $Le=10$ .

$Nb$	$-\theta'(0)$		$-\varphi'(0)$	
	Gorla and Chamkha [43]	Present results	Gorla and Chamkha [43]	Present results
0.1	0.3437461	0.3432	1.260950	1.2599
0.2	0.3210715	0.3208	1.321422	1.3200
0.3	0.2980915	0.2977	1.344729	1.3434
0.4	0.2761186	0.2757	1.359024	1.3574
0.5	0.2547152	0.2549	1.369532	1.3675

Excellent agreement between our results and published paper are found (**Tables 2 and 3**). These confirm the validity of the present MAPLE 18 methodology deployed. Note that comparisons are done for the case of quiescent free stream and for non-isothermal and non-solute plate conditions. It is important also to stress the need for a nanoparticle volume fraction *convective* boundary condition. While temperature convective conditions have been studied rigorously, the use of a mass convective condition has received less attention. This type of condition is important in certain biotechnological polymer flows and materials processing, as elaborated by Datta [58].

#### 4. NUMERICAL RESULTS AND DISCUSSION

Detailed **MAPLE 18** solutions have been plotted graphically to elucidate the impact of all key thermophysical parameters in **Figs. 2-18**, on the key flow characteristics i. e. velocity, temperature and nanoparticle volume fraction (concentration).

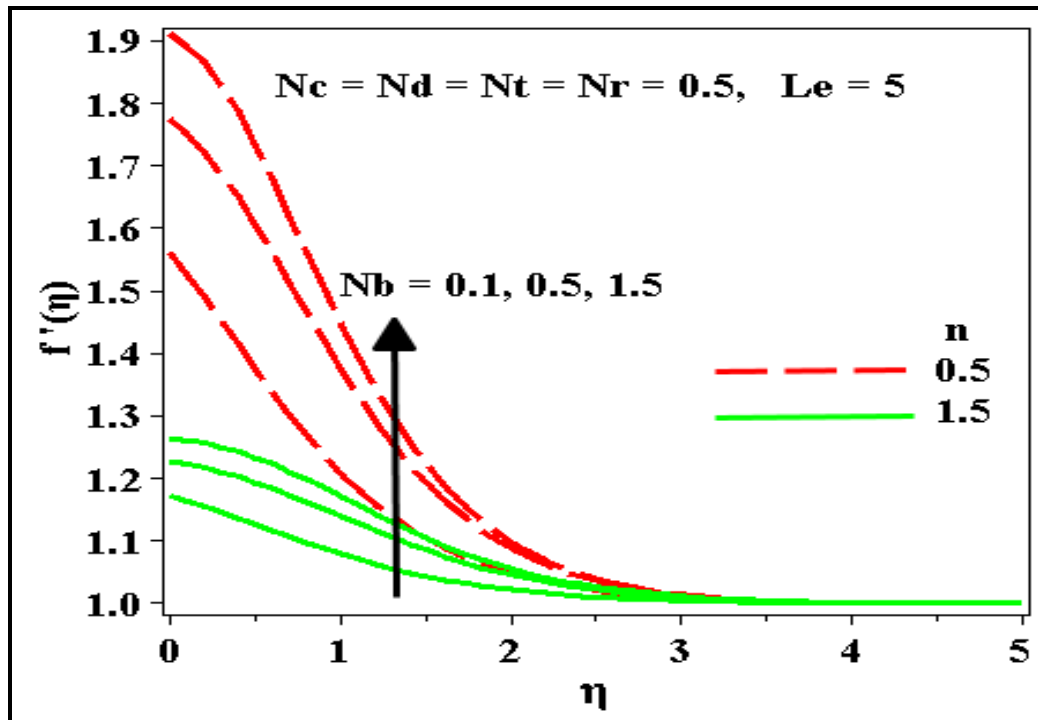


Fig.2. Effect of  $Nb$  on velocity with  $n$ .

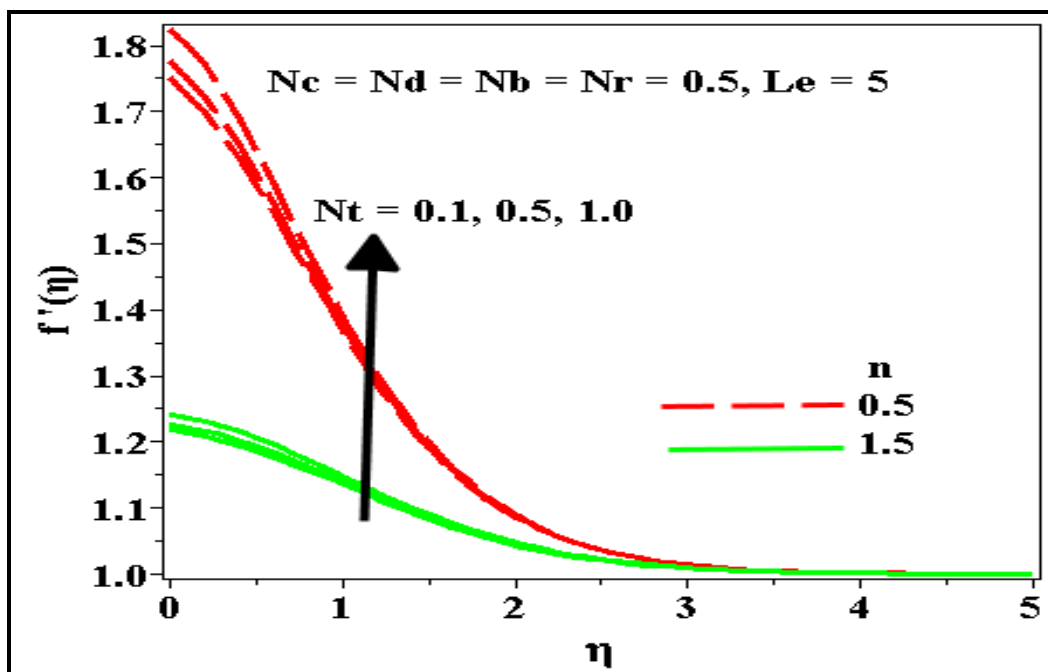


Fig.3. Effect of  $Nt$  on velocity profiles with  $n$ .

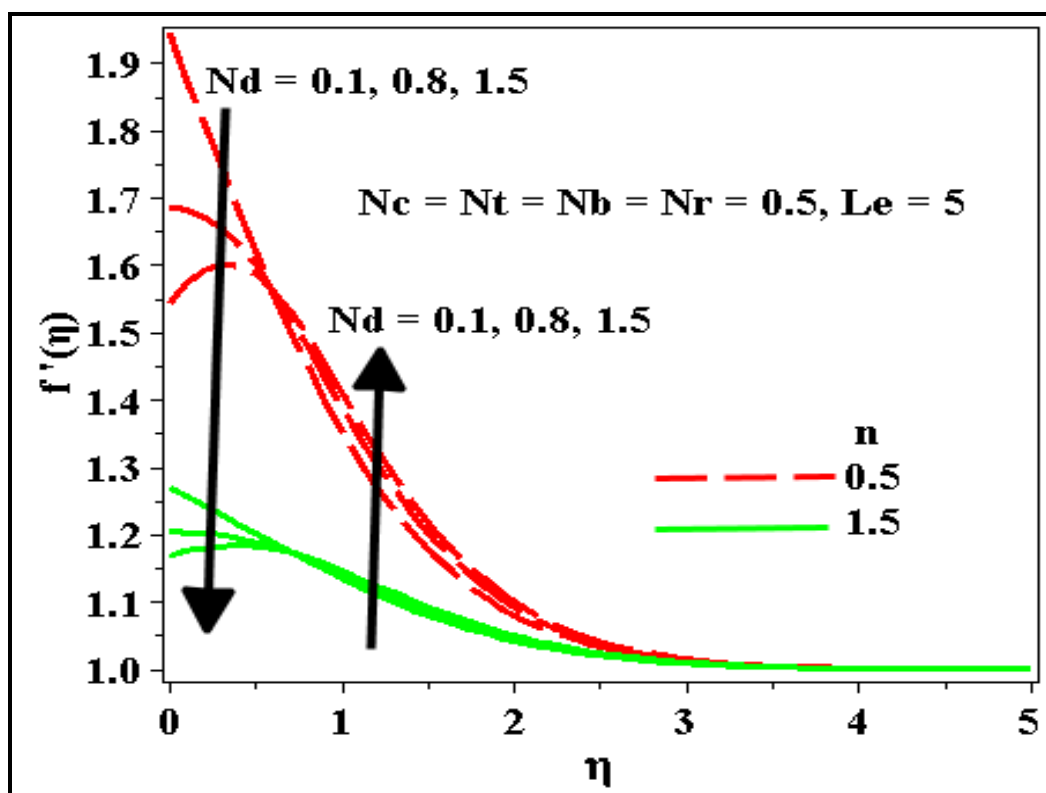


Fig.4. Effect of  $N_d$  on velocity with  $n$ .

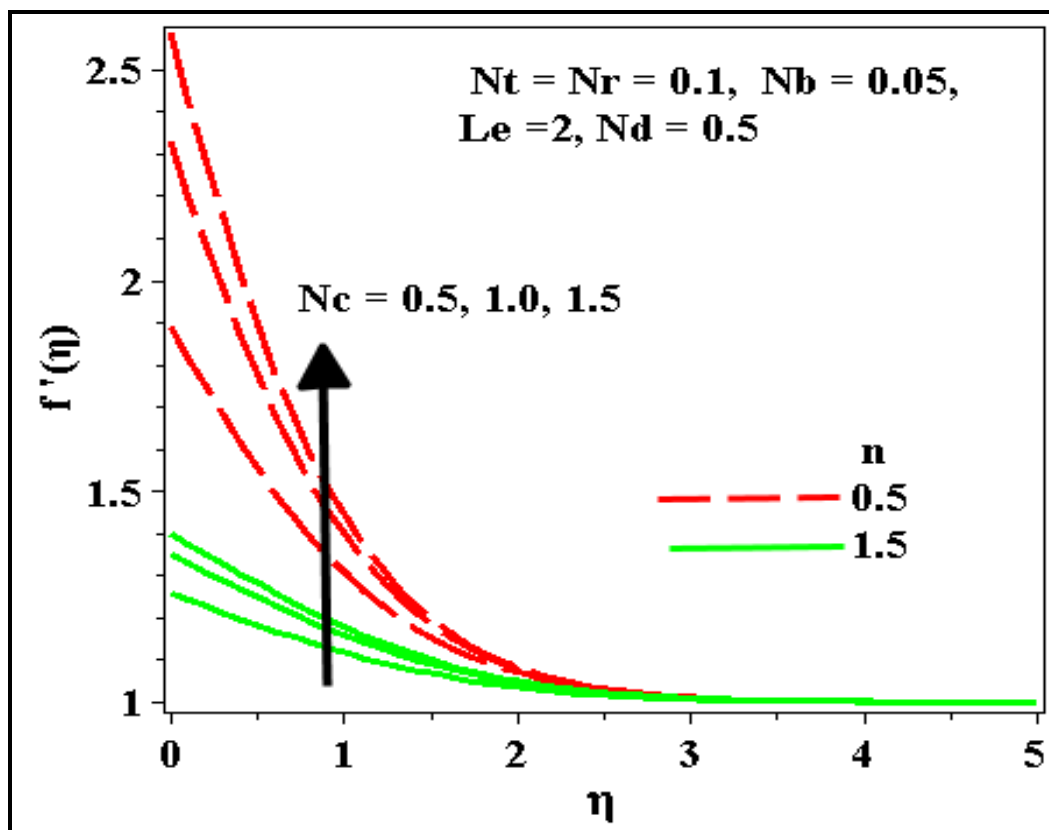


Fig.5. Effect of  $N_c$  on velocity with  $n$ .

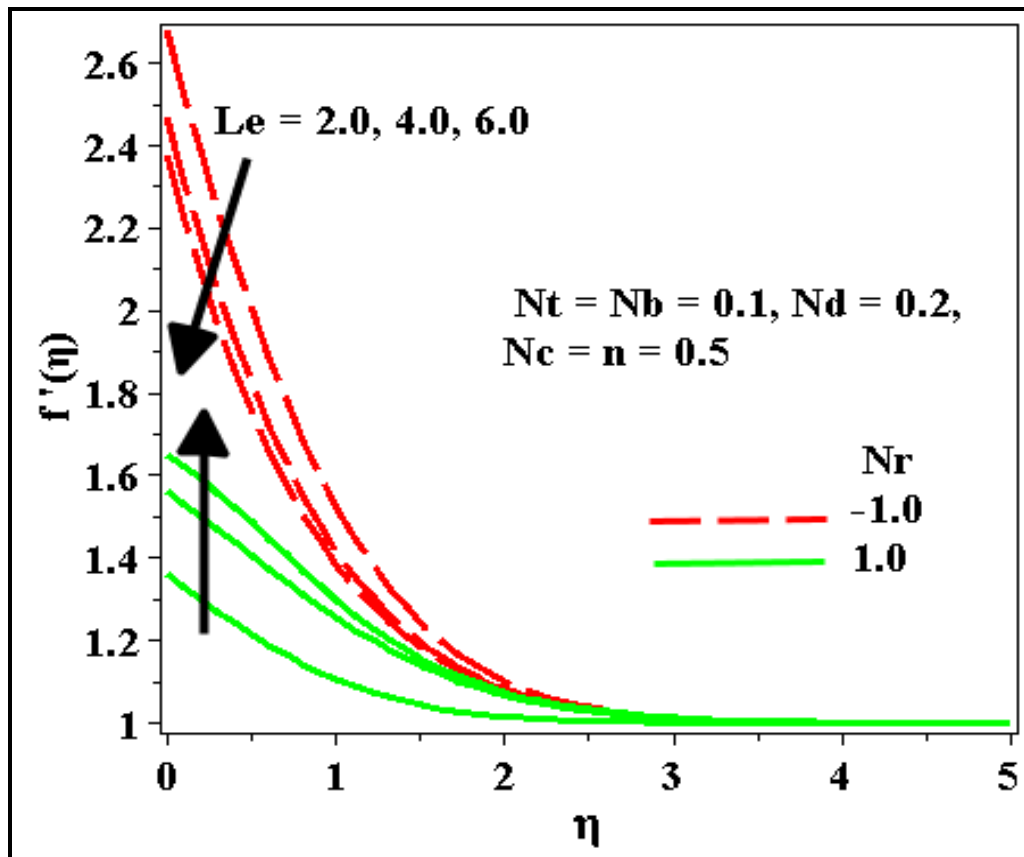


Fig.6. Effect of  $Le, Nr$  on velocity.

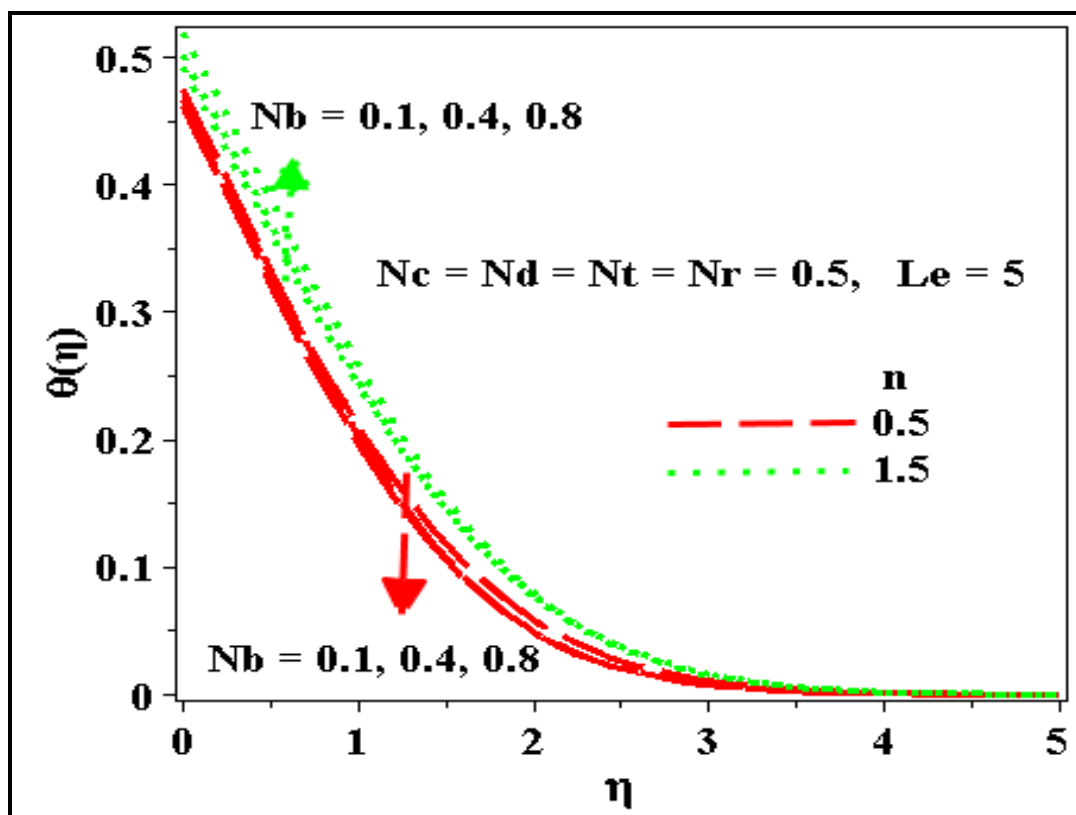


Fig.7. Effect of  $Nr$  and  $n$  on temperature.

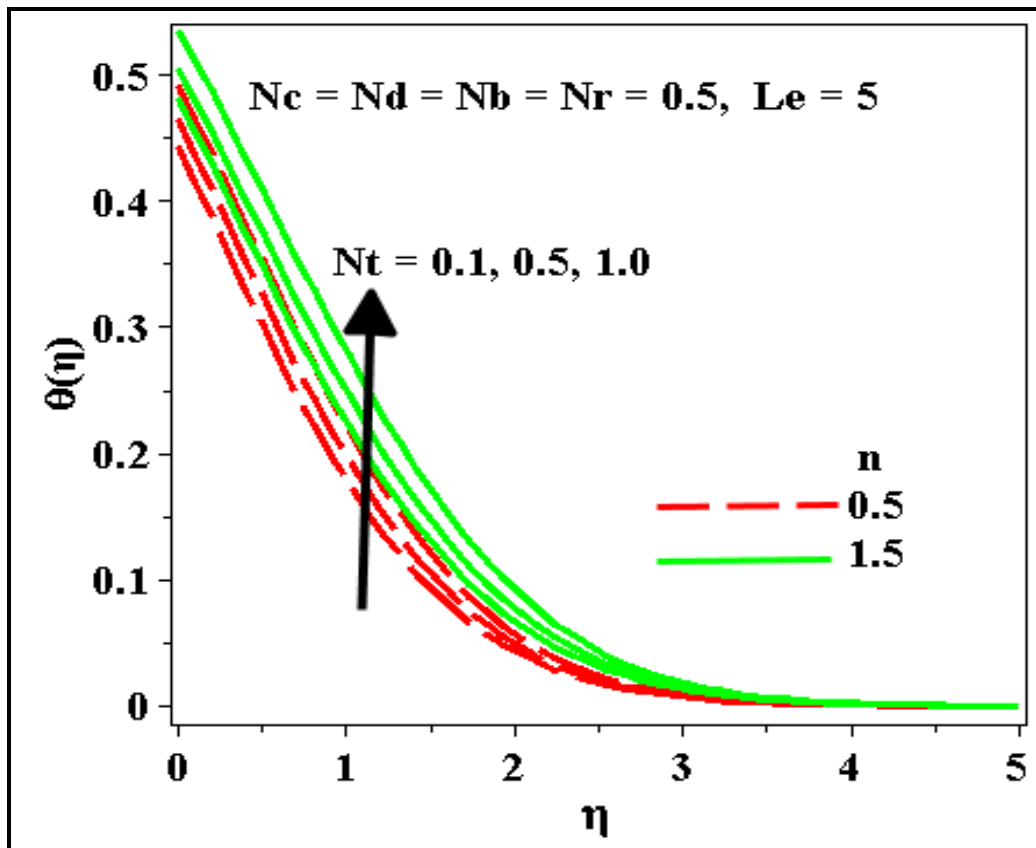


Fig. 8. Effect of  $Nt$  and  $n$  on temperature.

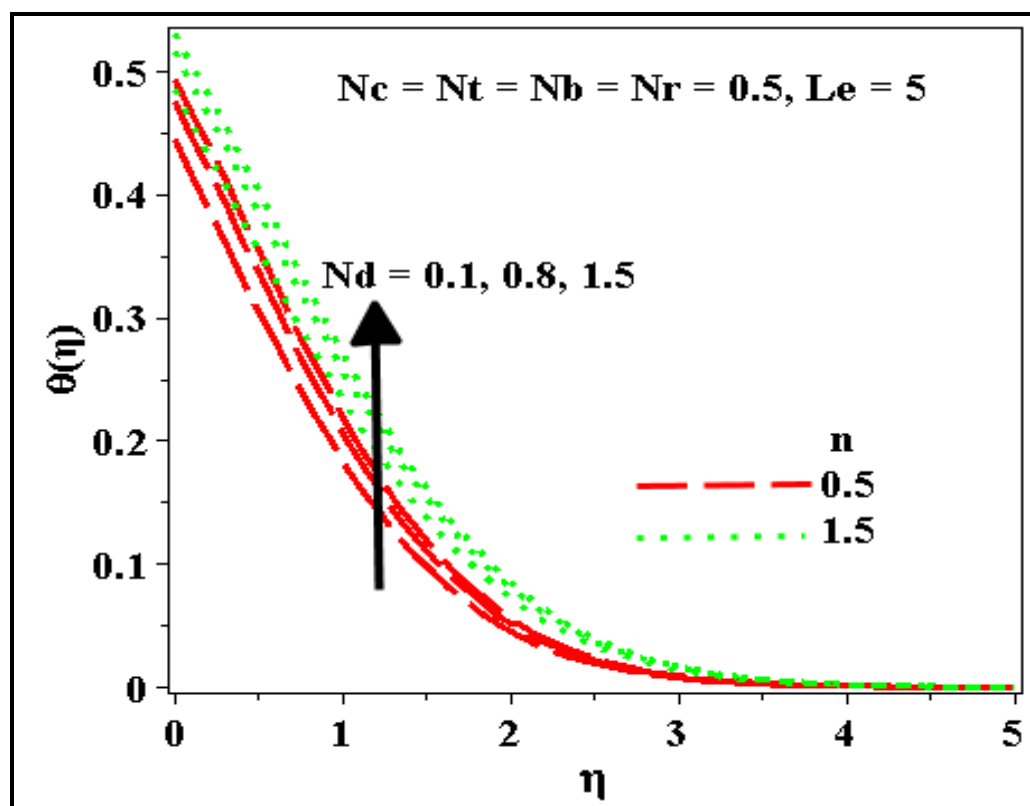


Fig.9. Effect of  $Nd$  and  $n$  on temperature.

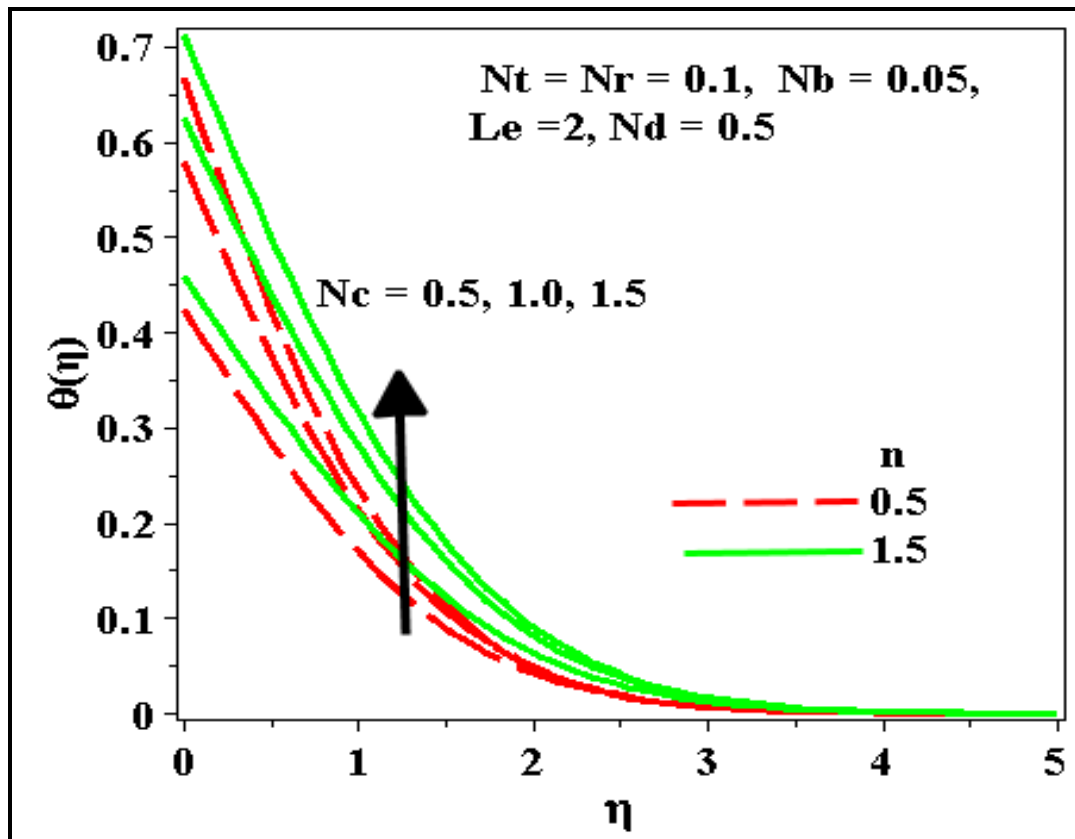


Fig.10. Effect of  $N_c$  and  $n$  on temperature.

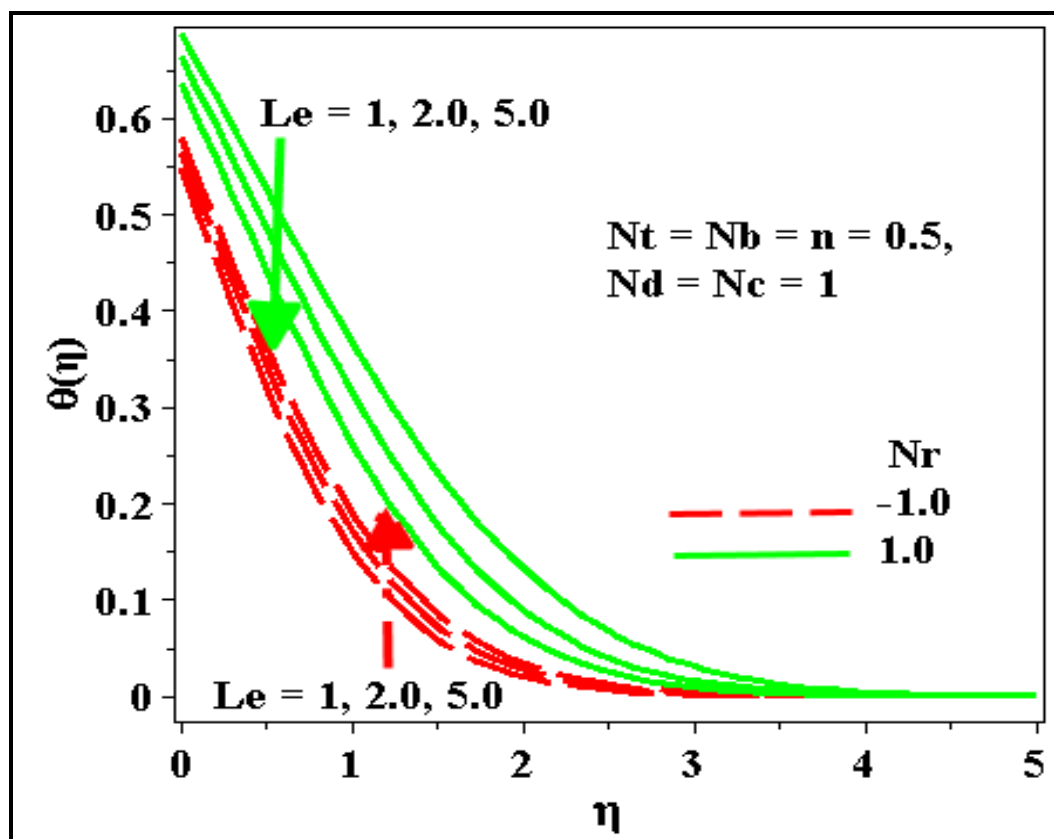


Fig.11. Effect of  $Le$  and  $n$  on temperature.

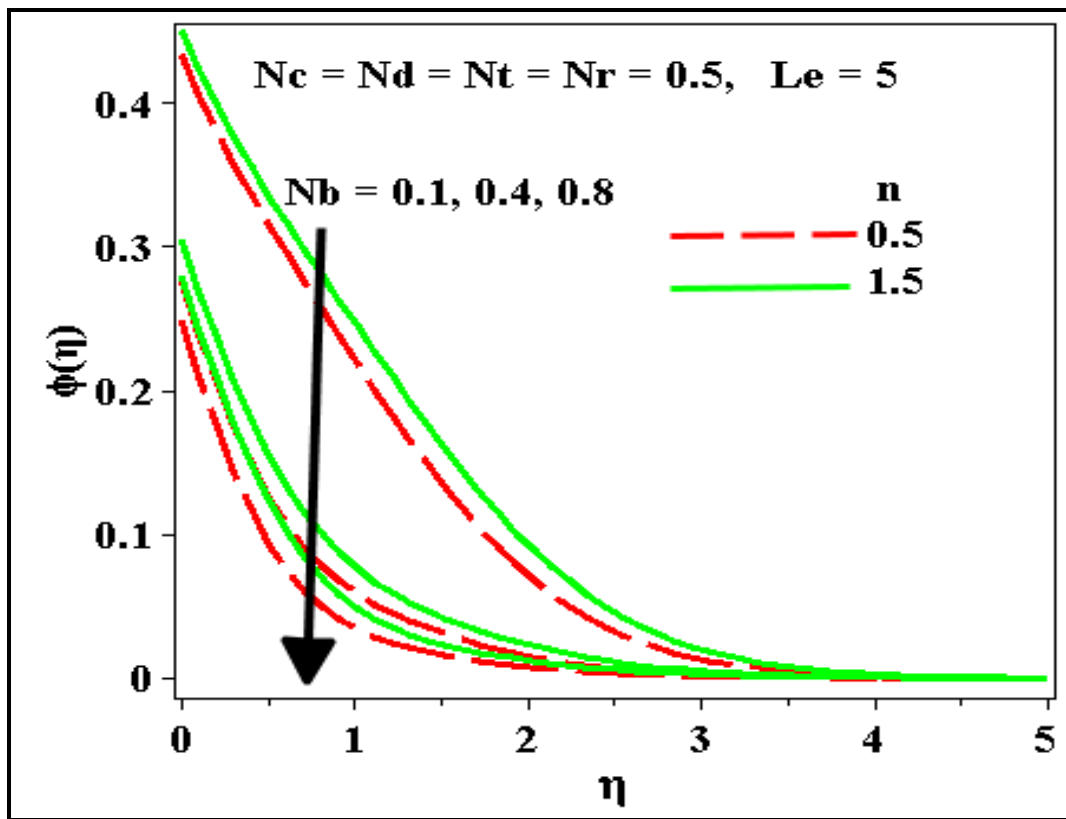
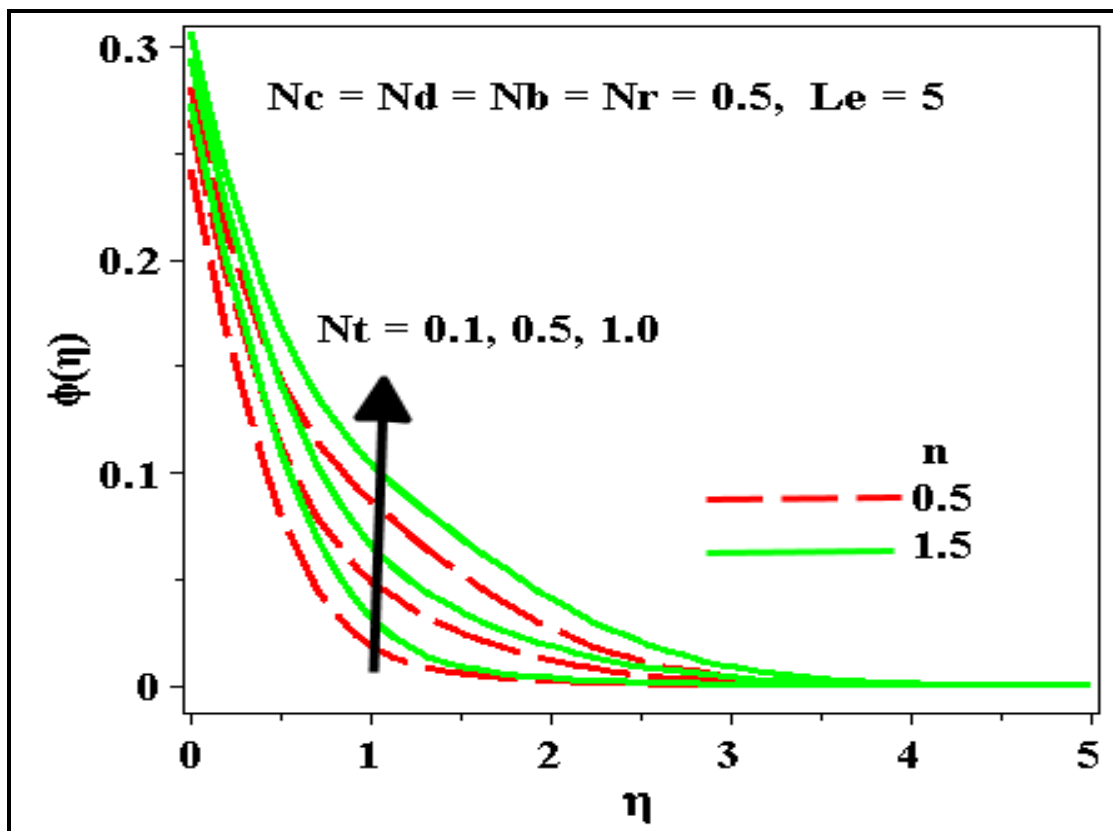
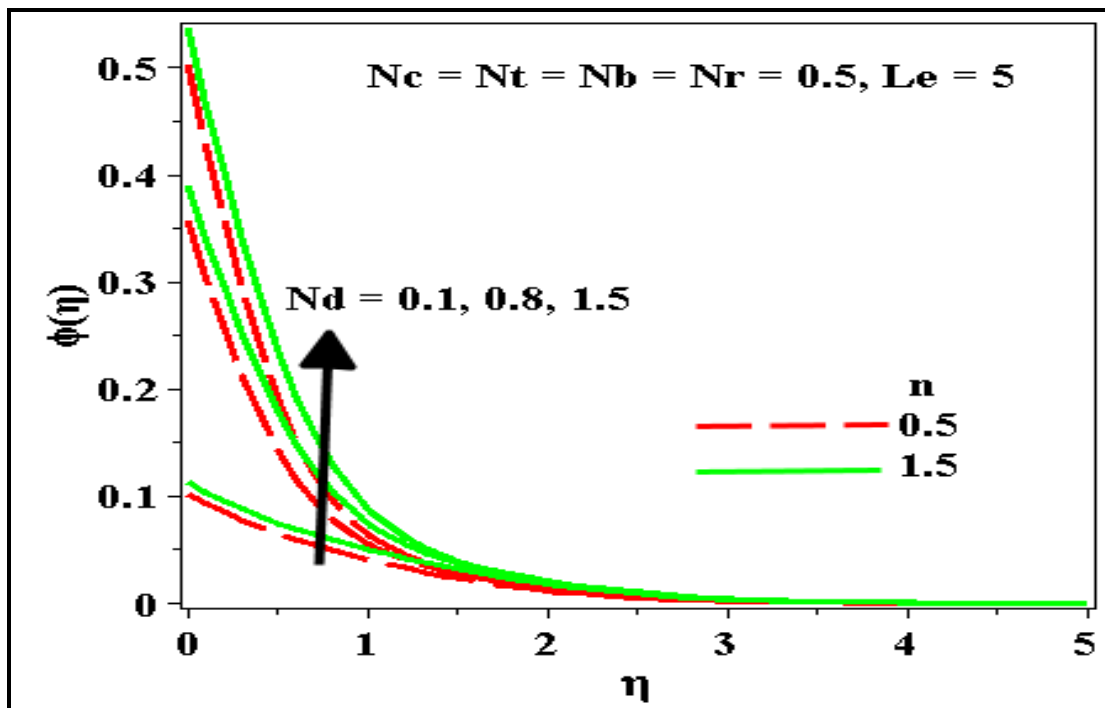


Fig.12. Effect of  $N_b$  and  $n$  on concentration.



**Fig.13.** Effect of  $N_t$  and  $n$  on nanoparticle volume fraction.



**Fig.14.** Effect of  $N_d$  and  $n$  on nanoparticle volume fraction.

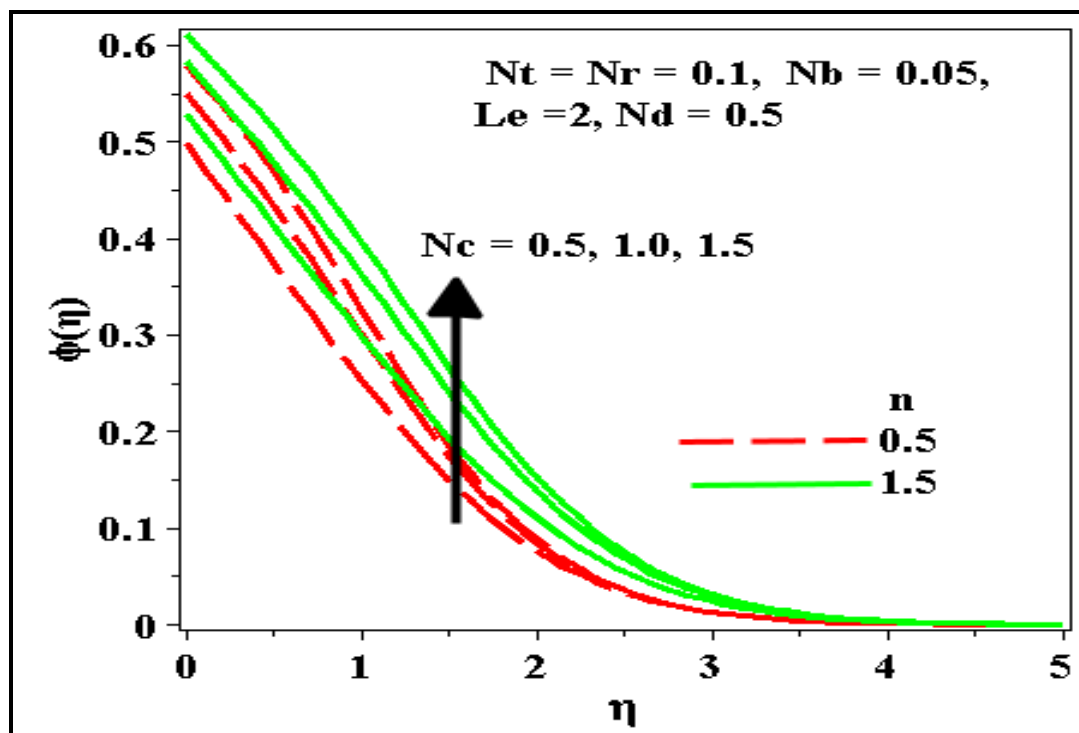


**Fig.15.** Effect of  $N_c$  and  $n$  on nanoparticle volume fraction.

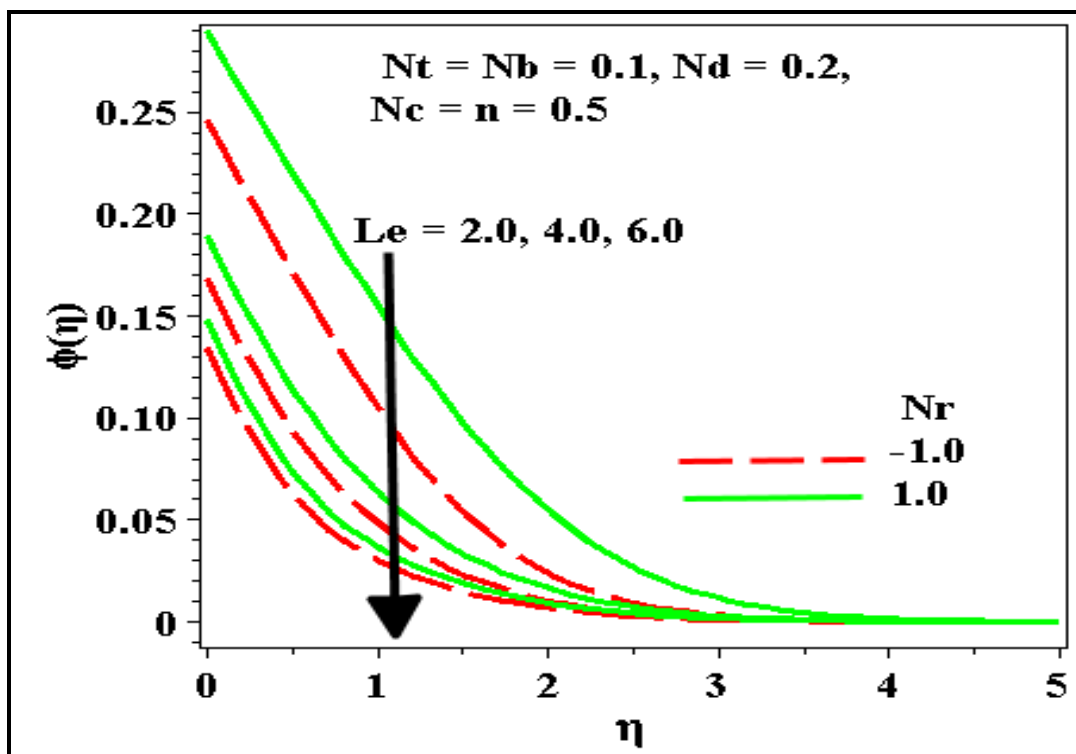


Fig.16. Effect of  $Le$  and  $Nr$  on nanoparticle volume fraction.

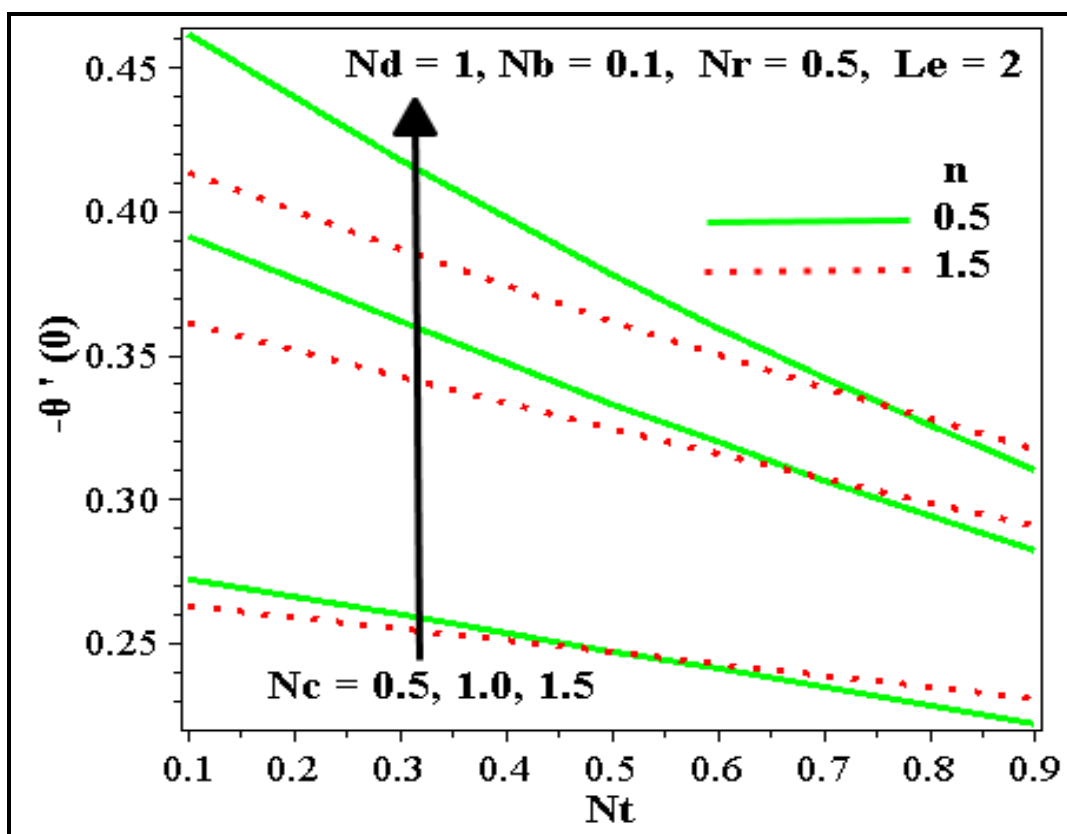
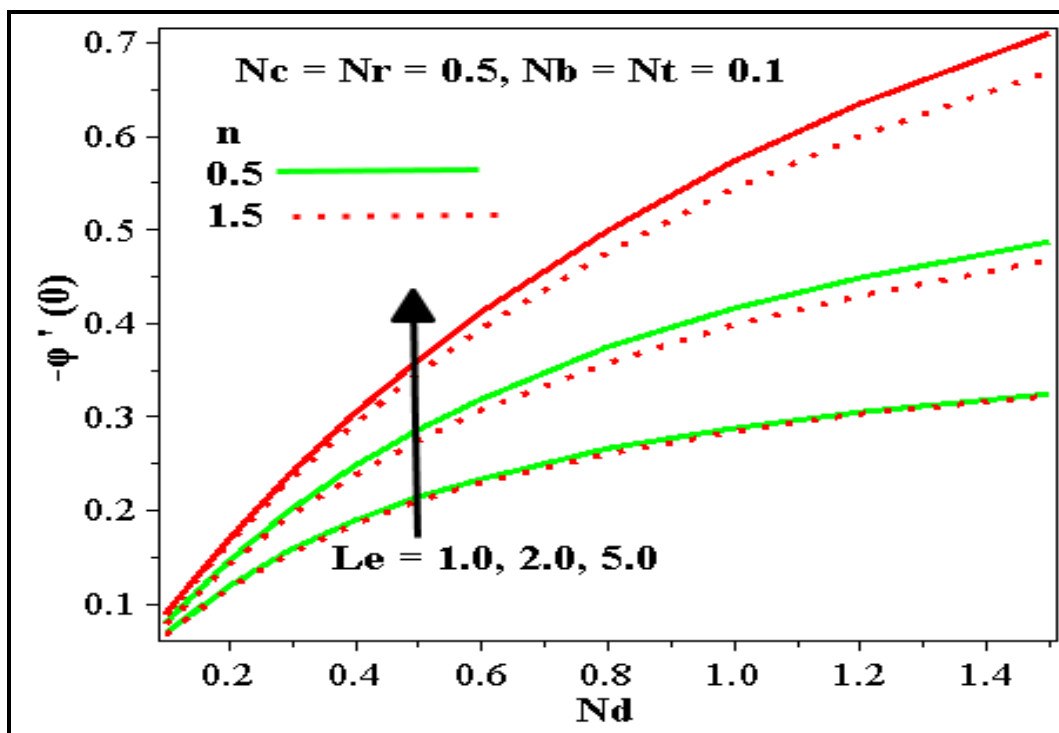


Fig.17. Effect of  $Nt$ ,  $n$  and  $Nc$  on reduced Nusselt number.



**Fig.18.** Effect of  $Nd$ ,  $n$  and  $Le$  on reduced Sherwood number.

Excellent correlation is achieved between the **MAPLE18** shooting solutions and the Chen and Chen [54] solutions which were obtained with a lower order shooting method. The present model reduces exactly to that of Chen and Chen by setting  $Nc = Nd \rightarrow \infty$ ,  $Nt \rightarrow 0$ ,  $Nb \rightarrow 0$ , and when nanoscale effects are negated i. e. nanoparticle volume fraction equation is discarded. Wall temperature gradients are observed to be significantly enhanced with a rise in  $n$ . Much higher temperature gradients are generated for dilatant fluids ( $n > 1$ ) as compared with pseudoplastic fluids. Therefore, even without *nanoscale* effects, dilatant fluids demonstrate improved thermal transport at the wall (substrate surface). **Table 2** shows also that the present **MAPLE18** computations concur well with the Blottner finite difference solutions for Newtonian nanofluid ( $n = 1$ ) of Gorla and Chamkha [43] for a wide range of buoyancy ratios ( $Nr$ ) in the absence of convective boundaries. Both heat and nanoparticle volume fraction gradient are found to be reduced with enhancing buoyancy ratio. Furthermore, in **Table 3**, again very good agreement is demonstrated with the solutions of Gorla and Chamkha [43] with various Brownian motion ( $Nb$ ) parameters. Temperature gradient is found to fall with rising  $Nb$  values whereas nanoparticle volume fraction gradient is strongly increased. An increment in  $Nb$  values in the Buongiorno model corresponds to smaller diameter nanoparticles which assist in species diffusion. This is important in actual fabrication of nanopolymers since the size of nanoparticles can be used to manipulate Brownian diffusion and hence the organization of nanoparticles throughout the coating.

#### 4.1 Dimensionless Velocity Behaviour

**Figures 2-6** demonstrate the influence of  $n$ ,  $Nb$ ,  $Nt$ ,  $Nd$ ,  $Nc$  and  $Le$  on the velocity. Note that  $Nc$  is essentially a *thermal Biot number* (ratio of the internal to boundary layer thermal resistance). In case of the nonappearance of  $Nc$  will lead to the left-face of the plate with the hot fluid to become completely insulated and the internal thermal resistance would be high. So, negligible amount of temperature gradient to the cold fluid on the right-face will occur. The convection-diffusion parameter  $Nd$  is similarly efficiently a *solutal Biot number*. It is apparent from **Figures 2-3** that  $Nb$  and  $Nt$  increase the velocity for both *pseudoplastic and dilatant nanofluids*; however, velocity is markedly greater for the pseudoplastic case since viscosity of the nanofluid is lower, as noted in [59]-[61]. Increasing Brownian motion effect is therefore beneficial to the boundary layer flow and accelerates it. Increasing thermophoretic effect, corresponding to enhanced particle deposition towards onto the vertical plate, is found to enhance momentum diffusion and accelerate the flow. **Figure 4** shows that with increasing convection-diffusion parameter,  $Nd$ , velocity for pseudoplastic nanofluids ( $n < 1$ ) whereas the contrary behaviour is induced in dilatant fluids ( $n > 1$ ). In the latter case, the flow is enhanced since with increasing the solutal Biot number i. e.  $Nd$ , there is an accompanying decrease in plate thermal resistance. Furthermore, stronger buoyancy forces are induced with greater convective-diffusion effect at the wall (plate) which encourage momentum development. **Figure 6** displays the consequence of Lewis number ( $Le$ ) on velocity for assisting/opposite buoyancies. Lewis number arises in the nanoparticle volume fraction (species) boundary layer eqn. (20). Lower  $Le$  values indicate a higher nanoparticle species diffusivity and a lower thermal diffusivity. For  $Le = 1$ , both diffusivities are equal. For  $Le < 1$ , species diffusion rate exceeds thermal diffusion rate, and vice versa for  $Le > 1$ . Here we examine the case for  $Le > 1$ . There is a important decrease in nanofluid velocity with increasing Lewis number, for the buoyancy-opposed scenario ( $Nr = -1$ ). The buoyancy force is featured in eqn. (18),  $+Nr\phi'$ , effectively coupling the momentum field to both the thermal and nanoparticle volume fraction fields, since  $Nr$  as defined in eqn. (12) expresses the ratio of species buoyancy force to thermal buoyancy force. For  $Nr < 0$ , the flow will therefore be accelerated, whereas for  $Nr > 0$  it will be decelerated. This is a classical result documented in numerous investigations, including Kaviany [18].

#### 4.2 Dimensionless Temperature Behaviour

**Figures. 7-11** illustrate the impact of the temperature field to variation in *power law index*  $n$ , *Brownian motion*  $Nb$ , *thermophoresis*  $Nt$ ,  $Nd$ ,  $Nc$ ,  $Le$ , and  $Nr$ . Increasing  $Nb$  (**fig. 7**) increases the temperature for dilatant nanofluids whereas it decreases it for pseudoplastic nanofluids. Clearly there is a connection between the viscosity of the nanofluid and the influence of Brownian motion. Chen *et al.* [44] have indicated that particle aggregate size, associated with Brownian motion, is influenced by the viscosity of the base fluid. For higher viscosity fluids ( $n = 1.5$  i.e., dilatant) thermal diffusion is enhanced and temperatures seem to be higher; the reverse is evident for pseudoplastic fluids. There is a more consistent response in temperature field however with increasing thermophoresis parameter,  $Nt$  and convection-diffusion parameter (nanoparticle volume fraction boundary parameter),  $Nd = (h_m)_o L / D_B Ra^{2n}$ , as observed in **figures 8-9**. In both cases temperature is increased, and thermal boundary layer thickness will also be enhanced. It is evident that dilatant nanofluids attain improved temperatures than pseudoplastic nanofluids which implies that in thermal management control, pseudoplastic nanopolymers achieve better cooling properties. **Figure 10** indicates that with a rise in  $Nc = (h_f)_o L / k Ra^{2n}$  which induces a decrease in thermal resistance of the plate, convective heat transfer to the fluid on the right-hand side of the plate is elevated. This will generate an escalation in temperatures; however, the pseudoplastic nanofluid again achieves lower temperatures than the dilatant nanofluid. The patterns observed in figure 10 show a strong agreement with the previous studies of for example, Khan and Gorla [62]. **Figure 11** illustrates that for pseudoplastic fluids ( $n = 0.5$ ), temperature is reduced with rising Lewis number,  $Le$ , for aiding buoyancy ( $Nr = 1$ ). This behaviour is attributable to a reduction in nanoparticles volume fractions since the nanoparticles volume fraction distribution is determined by temperature distribution. The opposite trend of temperature is witnessed in the case of opposing buoyancy ( $Nr = -1$ ).

#### **4.3 Dimensionless nanoparticle volume fraction (concentration) behaviour**

**Figures 12-16** depict the influence of  $n$ ,  $Nb$ ,  $Nt$ ,  $Nd$ ,  $Nc$ ,  $Le$ , and  $Nr$ , on the nanoparticle volume fraction are shown in. Increasing  $Nb$  serves to depress the concentration for dilatant nanofluids and pseudoplastic nanofluids (**Figure 12**), and magnitudes are higher for the former ( $n > 1$ ). Concentration increases with an increase in  $Nt$ ,  $Nd$  and  $Nc$  for both pseudoplastic and dilatant nanofluids, as revealed by **Figures 13-15**. In all cases, it is found that as with temperatures, nanoparticle volume fractions (concentrations) for dilatant

nanofluids are always more than those for pseudoplastic nanofluids which has a significant impact on the degree to which doping with homogeneity can be achieved in real nanopolymer manufacturing. **Figure 16** indicates that nanoparticle volume fraction is suppressed with increasing Lewis number for aiding buoyancy. The reason behind it, is that for a carrier fluid of given viscosity, the tiny value of the Brownian diffusion coefficient causes the nanoparticles concentration to decrease. These results again demonstrate good correlation with Gorla and Chamka [43].

#### ***4.4 Effects of the parameters on the heat and mass transfer rates***

**Figure 17** displays the consequence of  $Nt$ ,  $Nc$  on the reduced Nusselt number  $Shr$  for both pseudoplastic and dilatant nanofluids. It is found that  $Shr$  decreases with the thermophoresis parameter whereas they are boosted with the convection-conduction parameter. It is also found that the gradient of heat transfer of pseudoplastic nanofluid are greater in magnitude than the dilatant nanofluid. Finally, **figure 18** illustrates the effect of the Lewis number ( $Le$ ) and convection-diffusion parameter ( $Nd$ ) on the reduced Sherwood number for pseudoplastic and dilatant nanofluids. The nanoparticle volume fraction gradient rises with both Lewis number and convection-diffusion parameter. The nanoparticle volume fraction gradient of *pseudoplastic* nanofluids are also higher than those for the *dilatant* nanofluid. This implies that in nano-coating polymer flows enhanced mass transfer gradients can be produced more effectively with pseudoplastic nanofluid behaviour rather than with dilatant (shear thickening behaviour). In other words, nanoparticle diffusion effects, which will control the distribution of nanoparticles embedded in polymers can be manipulated effectively with the rheology of the nanopolymer. This in turn will influence the final constitution of the nanopolymer and bespoke designs may be fabricated for different industrial applications.

## **5. CONCLUSIONS**

A detailed theoretical and computational investigation of the steady two-dimensional free convective non-Newtonian nanofluid coating boundary layer flow along a plate located in a saturated isotropic Darcy environment. Appropriate scaling transformations is employed to derive the set of coordinate transformations and hence use them to find similar nonlinear boundary value problem before being solved by Maple 18 shooting quadrature method.

Excellent validation of computations with previous studies for special cases has been achieved. The principal observations from the present simulations can be summarized as follows:

- Temperature and nanoparticle volume fraction convective wall conditions with Brownian diffusion and thermophoresis in nanofluid coating flows have a considerable effect on the flow field and, hence on the heat and nanoparticle volume fraction gradient.
- Velocity, temperature, concentration as well as reduced nanoparticle (volume fraction) mass transfer rates increase with convective-diffusion parameter (solutal Biot number),  $Nd$ .
- Nusselt number increases with convective-conduction parameter,  $Nc$ , although it is suppressed with increasing power-law index,  $n$ , and thermophoresis parameter,  $Nt$ .
- Nanoparticle volume fraction rates are enhanced with Lewis number,  $Le$  and convective-diffusion parameter,  $Nd$  whereas they are substantially depleted with increasing power-law index,  $n$ .
- Velocity is reduced whereas temperature and nanoparticle volume fraction (concentration) are all elevated with  $n$ .
- Velocity, temperature, and nanoparticles volume fraction are all enhanced with convection-conduction parameter,  $Nc$ .
- Velocity is augmented whereas temperature is reduced with the rise in Lewis number,  $Le$ , for the buoyancy-assisted case ( $Nr > 0$ ). Furthermore, nanoparticle volume fraction decreases with  $Le$  for both aiding and opposing flow ( $Nr < 0$ ) cases.

The present paper can be extended to consider other non-Newtonian models (e.g. Oldroyd-B, micropolar, second and third grade Reiner-Rivlin differential viscoelastic models, micropolar fluid) for nanofluids. These formulations are under consideration and efforts in these directions will be communicated soon. Additionally future pathways may examine Williamson nanofluid rheology [63] and also consider alternative nanoscale models e.g. Tiwari-Das which enable an actual study of different metallic nanoparticles (copper, alumina) and also carbon nanotubes [64], ZnO-SAE50 nano-lubricants [65], magnetic nanoparticles [66, 67] viscoplastic nanofluids [68], Eyring-Powell nanofluids [69] and time-dependent nano-polymers [70].

## REFERENCES

- [1] S.U.S Choi, Nanofluids: from vision to reality through research, *ASME J. Heat Transfer*, 131, 1–9 (2009).
- [2] E. S. Day, J. G. Morton, J. L. West, Nanoparticles for thermal cancer therapy, *ASME J. Biomechanical Engineering*. 131(7), 074001 (2009).
- [3] D. Su, R. Ma, L. Zhu, Numerical study of nanofluid infusion in deformable tissues for hyperthermia cancer treatments, *Medical & Biological Engineering & Computing*, 49, 1233-1240 (2011).
- [4] M. J. Uddin, W. Khan, A. I. Md. Ismail, Free convective flow of non-Newtonian nanofluid in porous media with gyrotactic microorganisms, *AIAA J. Thermophysics and Heat Transfer* (2013). <https://doi.org/10.2514/1.T3983>
- [5] A. V. Kuznetsov, Nanofluid bioconvection: interaction of microorganisms oxytactic upswimming, nanoparticle distribution, and heating/cooling from below, *Theoretical and Computational Fluid Dynamics*, 26, 291-310 (2012).
- [6] O. Anwar Bég, Nanoparticle-doped rocket gel propellants – modelling of enhanced combustion properties using CFD, *Technical Report- Aero-3-3-13, 135 pages, Gort Engovation Research, Bardford, UK, February* (2013).
- [7] R. Di Paola, R. Savino, D. Mirabile Gattia, R. Marazzi, M. Vittori Antisari, Self-rewetting carbon nanofluid as working fluid for space and terrestrial heat pipes, *J. Nanoparticle Research*, 13, 6207-6216 (2011).
- [8] P. Rana, O. Anwar Bég and R. Bhargava, Finite element modelling of conjugate mixed convection flow of Al-water nanofluid from an inclined slender hollow cylinder, *Physica Scripta*, 88 (2013) (15pp).
- [9] T. Parametthanuwat, S. Rittidech, A. Pattiya, Y. Ding, S. Witharana, Application of silver nanofluid containing oleic acid surfactant in a thermosyphon economizer, *Nanoscale Research Letters*, 6, 315 (2011).
- [10] H. Abbassi and C. Aghanajafi, Evaluation of heat transfer augmentation in a nanofluid-cooled microchannel heat sink, *J. Fusion Energy*, 25, 187-196 (2006).
- [11] R. Ellahi, M. Raza and V. Vafai, Series solutions of non-Newtonian nanofluids with Reynolds' model and Vogels' model by means of the homotopy analysis method, *Mathematical and Computer Modelling*, 55, 1876-1891 (2012).
- [12] D.A. Nield, A note on the onset of convection in a layer of a porous medium saturated by a non-Newtonian nanofluid of power-law type, *Transport in Porous Media*, 87, 121- 123, (2011).
- [13] M. Hojjat, S.G.H. Etemad, R. Bagheri and J. Thibault, Convective heat transfer of non-Newtonian nanofluids through a uniformly heated circular tube, *Int. J. Thermal Sciences*, 50, 525-531 (2011).
- [14] P. Rana, R. Bhargava, O. Anwar Bég and A. Kadir, Finite element analysis of viscoelastic nanofluid flow with energy dissipation and internal heat source/sink effects, *Int. J. Applied Computational Mathematics*, 3 (2) 1421–1447 (2017).
- [15] M.A. Rashad, M.A. El-Hakim and M.M.M. Abdou, Natural convection boundary layer of a non-Newtonian fluid about a permeable vertical cone embedded in a porous medium saturated with a nanofluid, *Computers & Mathematics with Applications*, 62, 3140-3151 (2011).
- [16] L.J. Sheu, H-S Chiou, W-T Weng and S-R Lee, The onset of convection in a viscoelastic nanofluid layer, *Int. Conf. Electronic and Mechanical Engineering and Information Technology (EMEIT), Taiwan, August* (2011).
- [17] R. Chand and G.C. Rana, Thermal instability of Rivlin-Ericksen elastic-viscous nanofluid flow in a saturated porous medium, *ASME J. Fluids Eng.* 134, 121203 (2012).

- [18] M. Kaviany, *Principles of Heat Transfer in Porous Media*, Second Edition, Springer-Verlag, New York (1999).
- [19] P M Adler, and H Brenner, Multiphase flow in porous media, *Annual Review of Fluid Mechanics*, 20, 35-59 (1988).
- [20] M. A. Mujeebu, M. Z. Abdullah, A.A. Mohamad and M.Z. Abu Bakar, Trends in modeling of porous media combustion, *Progress in Energy and Combustion Science*, 36, 627-650 (2010).
- [21] O. Anwar Bég, J. Zueco and S.K. Ghosh, Unsteady hydromagnetic natural convection of a short-memory viscoelastic fluid in a non-Darcian regime: network simulation, *Chemical Engineering Communications*, 198, 172-190 (2011).
- [22] A.V. Shenoy, Non-Newtonian fluid heat transfer in porous media, *Advances in Heat Transfer*, 2, 101-190 (1994).
- [23] O. Anwar Bég, H.S. Takhar, J. Zueco, A. Sajid and R Bhargava, Transient Couette flow in a rotating non-Darcian porous medium parallel plate configuration: network simulation method solutions, *Acta Mechanica*, 3, 129-144 (2008).
- [24] O. Anwar Bég., Bhargava, R., Rawat, S., and Kahya, E., Numerical study of micropolar convective heat and mass transfer in a non-Darcian porous regime with Soret/Dufour diffusion effects, *Emirates J. Eng. Res.*, **13**, 51–66 (2008).
- [25] M. M. Rashidi, M. Keimanesh, O. Anwar Bég and T.K. Hung, Magnetohydrodynamic bio-rheological transport phenomena in a porous medium: A simulation of magnetic blood flow control and filtration, *Int. J. Num. Meth. Biomedical Engineering*, 27, 805-821 (2011).
- [26] O. Anwar Bég and J. Zueco, Network numerical simulation applied to pulsatile non-Newtonian flow through a permeable medium channel with couple stress and wall mass flux effects, *Int. J. Appl. Math. Mechanics*, 5, 1-16 (2009).
- [27] L.B. Younis and R. Viskanta, Experimental determination of the volumetric heat transfer coefficient between stream of air and ceramic foam, *Int. J. Heat Mass Transfer*, 36, 1993, 1425–1434 (1993).
- [28] O. Anwar Bég and O.D. Makinde, Viscoelastic flow and species transfer in a Darcian high-permeability channel, *J. Petroleum Science and Engineering*, 76, 93-99 (2011).
- [29] O. Anwar Bég, J. Zueco and H.S. Takhar, Laminar free convection from a continuously-moving vertical surface in thermally-stratified non-Darcian high-porosity medium: Network numerical study, *Int. Comm. Heat Mass Transfer*, 35, 810-816 (2008).
- [30]. P. Cheng and W.J. Minkowycz, Free convection about a vertical flat plate embedded in a porous medium with application to heat transfer from a dike, *J. Geophysical Research*, 82, 2040-2044 (1977).
- [31] M. Mahmoud, Numerical solution of free-convection heat transfers over a vertical cone embedded in a non-Newtonian power-law fluid-saturated porous medium with viscous dissipation, *ASCE J. Engineering Mechanics*, 138, 555–559 (2012).
- [32] D. Tripathi and O. Anwar Bég, Magnetohydrodynamic peristaltic flow of a couple stress fluid through coaxial channels containing a porous medium, *J. Mech. Med. Biol.*, 12, 1250088.1-1250088.20 (2012).
- [33] O. Anwar Bég, Tasveer Bég, R. Bhargava, S. Rawat and D. Tripathi, Finite element study of transient pulsatile magneto-hemodynamic non-Newtonian flow and drug diffusion in a porous medium channel, *J. Mech. Med. Biol.*, 12, 1250081.1-1250081.26 (2012).
- [34] O. Anwar Bég, Tasveer Bég, Takhar HS, Raptis A, Mathematical and numerical modeling of non-Newtonian thermo-hydrodynamic flow in non-Darcy porous media, *Int. J. Fluid Mechanics Research*, 31, 1-12 (2004).
- [35] O. Anwar Bég, Takhar HS, Bhargava R, Rawat S, Prasad VR, Numerical study of heat transfer of a third-grade viscoelastic fluid in non-Darcian porous media with thermophysical effects, *Physica Scripta*, 77, 1-11 (2008).

- [36] J. Zueco, O. Anwar Bég, H.S. Takhar, Network numerical analysis of magneto-micropolar convection through a vertical circular non-Darcian porous medium conduit, *Computational Materials Science*, 46, 1028-1037 (2009).
- [37] V.R. Prasad, B. Vasu, O. Anwar Bég and R. Prashad, Unsteady free convection heat and mass transfer in a Walters-B viscoelastic flow past a semi-infinite vertical plate: numerical study, *Thermal Science*, 15, S2, S291-S305 (2011).
- [38] S. Wang, B. Yu, A fractal model for the starting pressure gradient for Bingham fluids in porous media embedded with fractal-like tree networks, *Int. J. Heat Mass Transfer*, 54, 4491-4494 (2011).
- [39] D. Tripathi and O. Anwar Bég, A numerical study of oscillating peristaltic flow of generalized Maxwell viscoelastic fluids through a porous medium, *Transport in Porous Media*, 95, 337-348 (2012).
- [40] T. A. Bég, M. M. Rashidi, O. Anwar Bég and N. Rahimzadeh, Differential transform semi-numerical analysis of biofluid-particle suspension flow and heat transfer in non-Darcian porous media, *Computer Methods in Biomechanics and Biomedical Engineering* (2012). DOI:10.1080/10255842.2011.643470
- [41] D.A. Nield, A.V. Kuznetsov, The Cheng–Minkowycz problem for natural convective boundary layer flow in a porous medium saturated by a nanofluid, *Int. J. Heat and Mass Transfer*, 52, 5792–5795 (2009).
- [42] A. Aziz, A similarity solution for laminar thermal boundary layer over a flat plate with a convective surface boundary condition, *Communication in Nonlinear Science and Numerical Simulation*, 14, 1064–1068 (2009).
- [43] R.S.R. Gorla and A. Chamkha, Natural convective boundary layer flow over a nonisothermal vertical plate embedded in a porous medium saturated with a nanofluid, *Nanoscale and Microscale Thermophysical Engineering*, 15, 81-94 (2012).
- [44] Haisheng Chen *et al*, Rheological behaviour of nanofluids, *New J. Phys.* 9 367 (2007).
- [45] R. Seshadri and T.Y. Na, *Group Invariance in Engineering Boundary Value Problems*, Springer-Verlag, New York (1985).
- [46] N.H. Ibragimov, *Lie Group Analysis of Differential Equations*, CRC, Press Boca Raton, U.S.A. (1994).
- [47] Md Jashim Uddin, N H Md Yusoff, O Anwar Bég and Ahamd Izani Ismail, Lie group analysis and numerical solutions for non-Newtonian nanofluid flow in a porous medium with internal heat generation, *Phys. Scr.* 87, 1-14 (2013).
- [48] B. Lindgren, J.M. Osterlund, A. V. Johansson, Evaluation of scaling laws derived from Lie group symmetry methods in zero-pressure-gradient turbulent boundary layers, *J. Fluid Mechanics*, 502, 127-152 (2004).
- [49] A.A. Afify and N.S. Elgazery, Lie group analysis for the effects of chemical reaction on MHD stagnation-point flow of heat and mass transfer towards a heated porous stretching sheet with suction or injection, *Nonlinear Analysis: Modelling and Control*, 17, 1-15 (2012).
- [50] M. Oberlack, A.F. Cheviakov, Higher-order symmetries and conservation laws of the G-equation for premixed combustion and resulting numerical schemes, *J. Eng. Maths.*, 66, 121-140 (2010).
- [51] M.J. Uddin, W.A. Khan and A.I.M. Ismail, Free convection boundary layer flow from a heated upward facing horizontal flat plate embedded in a porous medium filled by a nanofluid with convective boundary condition, *Transport in Porous Media*, 92, 867-881 (2012).
- [52] M. Ferdows, M.J. Uddin and A.A. Afify, Scaling group transformation for MHD boundary layer free convective heat and mass transfer flow past a convectively heated nonlinear radiating stretching sheet, *Int. J. Heat and Mass Transfer*, 56, 181–187 (2013).

- [53] A. Aziz A, M.J. Uddin, M.A.A. Hamad and A.I.M. Ismail, MHD flow over an inclined radiating plate with the temperature-dependent thermal conductivity, variable reactive index, and heat generation, *Heat Transfer-Asian Research*, 41, 241-259 (2012)..
- [54]. H.T. Chen and C.K. Chen, Free convection flow of non-Newtonian fluids along a vertical plate embedded in a porous medium, *ASME J. Heat Transfer*, 110, 257-260 (1988).
- [55] V. Srivastava, D. Tripathi and O. Anwar Bég, Numerical study of oxygen diffusion from capillaries to tissues with external force effects, *J. Mechanics in Medicine and Biology*, 17, No. 2 (2016) 1750027 (20 pages).
- [56] O. Anwar Bég, M.J. Uddin, Tasveer A. Bég, Ali Kadir, M Shamsuddin, M. Babaie. Modelling mass transfer from a rotating cone in anisotropic porous media with Stefan blowing and Navier slip, *Indian J. Physics* (2019) doi.org/10.1007/s12648-019-01520-9 (16 pages)
- [57] J. P. Denier and P. P. Dabrowski, On the boundary-layer equations for power-law fluids, *Proc. R. Soc. Lond. A*, 460, 3143–3158 (2004).
- [58] A.K. Datta, Heat Transfer, in *Handbook of Food and Bioprocess Modelling Techniques*, CRC, Florida, (2006).
- [59] Rudyak, V., & Krasnolutskkii, S. L., Dependence of the viscosity of nanofluids on nanoparticle size and material. *Physics Letters A*, 378, 26-27 (2014)
- [60] Jamal-Abad, M. T., Dehghan, M., Saedodin, S., Valipour, M. S., & Zamzamian, A., An experimental investigation of rheological characteristics of non - Newtonian nanofluids. *Journal of Heat and Mass Transfer Research*, 1, 17-23 (2013).
- [61] Hojjat, M., Etemad, S. G., Bagheri, R., & Thibault, J., Rheological characteristics of non-Newtonian nanofluids: Experimental investigation. *International Communications in Heat and Mass Transfer*, 38(2) (2011).
- [62] W.A. Khan and R.S.R. Gorla, Heat and mass transfer in power-law nanofluids over a non-isothermal stretching wall with convective boundary condition, *ASME J. Heat Transfer* 134, 112001 (2012).
- [63] P.C. Pattanaik et al., Impact of radiative and dissipative heat on the Williamson nanofluid flow within a parallel channel due to thermal buoyancy, *Proceedings of the Institution of Mechanical Engineers, Part N: Journal of Nanomaterials, Nanoengineering and Nanosystems*, 2022. <https://doi.org/10.1177/23977914221080046>
- [64] P.K. Pattanaik et al Analysis of Metallic Nanoparticles (Cu, Al<sub>2</sub>O<sub>3</sub>, and SWCNTs) on Magnetohydrodynamics Water-Based Nanofluid through a Porous Medium, *Journal of Mathematics*, 2022. <https://doi.org/10.1155/2022/3237815>
- [65] M.K. Nayak et al., Magnetohydrodynamic flow and heat transfer impact on ZnO-SAE50 nanolubricant flow over an inclined rotating disk, *J. Central South University*, Volume 26, pages 1146–1160, (2019)
- [66] R. Mehmood et al., Radiative slip transport of magnetized gyrotactic micro-organisms submerged with nano fluid along a vertical stretching surface with suction/injection effects, *Proceedings of the Institution of Mechanical Engineers, Part N: Journal of Nanomaterials, Nanoengineering and Nanosystems* <https://doi.org/10.1177/23977914231176866> (2023).
- [67] S.A. Shehzad et al., Regression analysis of horizontal magnetic field in slippery nanofluid flow with Arrhenius activation energy, *Journal of Molecular Liquids*, 392, 123522 (2023).

[68] H.B. Lanjwani *et al.*, Stability analysis of stratified radiative non-Newtonian Casson nanofluid flow past on stretching/shrinking sheet using two-phase model, *Chinese Journal of Physics*, 85, 752-775 (2023).

[69] N. Anum *et al.* Numerical analysis for thermal performance of modified Eyring Powell nanofluid flow subject to activation energy and bioconvection dynamic, *Case Studies in Thermal Engineering*, 39, 102427 (2022).

[70] Z. Hussain and W.A. Khan, Impact of thermal-solutal stratifications and activation energy aspects on time-dependent polymer nanoliquid, *Waves in Random and Complex Media* (2022). <https://doi.org/10.1080/17455030.2022.2128229>